

1 **Evolutionary metabolomics of specialized metabolism diversification in the genus *Nicotiana***
2 **highlights allopolyploidy-mediated innovations in *N*-acylnornicotine metabolism**

3
4 **Authors:** David Elser¹, David Pflieger¹, Claire Villette¹, Baptiste Moegle², Laurence Miesch² and
5 Emmanuel Gaquerel^{1,*}

6
7 **Affiliations:**

8 ¹Institut de Biologie Moléculaire des Plantes du CNRS, Université de Strasbourg

9 ²Institut de Chimie du CNRS UMR 7177, Université de Strasbourg

10
11 ***Corresponding author:**
12 Emmanuel Gaquerel
13 Institut de Biologie Moléculaire des Plantes du CNRS, Université de Strasbourg, 12 rue du
14 Général Zimmer, 67084 Strasbourg Cedex France
15 E-mail address: emmanuel.gaquerel@ibmp-cnrs.unistra.fr
16 Tel: +33 (0)367155352

17
18 **E-mail addresses:**
19 DE, delser@unistra.fr; DP, david.pflieger@ibmp-cnrs.unistra.fr; CV, claire.villette@ibmp-
20 cnrs.unistra.fr; BM, bmoegle@unistra.fr; LM, lmiesch@unistra.fr; EG,
21 emmanuel.gaquerel@ibmp-cnrs.unistra.fr

22
23

24 **Abstract**

25 Specialized metabolite (SM) diversification is a core process to plants' adaptation to diverse
26 ecological niches. Here we implemented a computational mass spectrometry (MS)-based
27 metabolomics approach to explore SM diversification in tissues of 20 species covering *Nicotiana*
28 phylogenetics sections. To drastically increase metabolite annotation, we created a large *in silico*
29 fragmentation database, comprising more than 1 million structures, and scripts for connecting
30 class prediction to consensus substructures. Altogether, the approach provides an unprecedented
31 cartography of SM diversity and section-specific innovations in this genus. As a case-study, and
32 in combination with NMR and MS imaging, we explored the distribution of *N*-acyl nornicotines,
33 alkaloids predicted to be specific to *Repandae* allopolyploids, and revealed their prevalence in the
34 genus, albeit at much lower magnitude, as well as a greater structural diversity than previously
35 thought. Altogether, the novel data integration approaches provided here should act as a resource
36 for future research in plant SM evolution.

37

38 **Keywords:** Computational metabolomics, plant specialized metabolism, chemodiversification,
39 *N*-acylnornicotines

40

41 **Teaser:** Computational metabolomics delineates main trends in the diversification of specialized
42 metabolism in the genus *Nicotiana*

43

44

45 Introduction

46 Plant metabolic profiles represent complex traits that reflect both evolutionary and temporally
47 dynamic adaptations to specific ecological niches. Compared with their counterparts integrated
48 into broadly conserved central C metabolism pathways, specialized metabolites (SMs) contribute
49 to the largest fraction of inter-specific variations in plant metabolic profiles. This plant
50 chemodiversity is predicted to account for somewhere on the order of one hundred thousand to
51 one million chemically unique structures, with an estimated range of five thousand to fifteen
52 thousand structures *per* plant species (1). Many of these SMs act as chemical shields or as
53 attractants in plant biotic interactions. In this respect, a relatively recent paradigm shift as part of
54 ecological hypotheses such as the synergy (2) and interaction diversity hypotheses (3), has been to
55 consider SM structural diversity, and not solely the summation of individual metabolites, as a
56 critical determinant of plants' ecological interactions. The latter perspective also revives the
57 interest in the exploration of SM diversity with modern analytical approaches and the use of
58 adequate statistical descriptors (4).

59 In analogy to phylogenomics approaches that have flourished as a result of both the
60 increasing release of annotated genomes and of established comparative bioinformatics pipelines
61 to analyze these data, recent years have indeed seen a resurgence of plant family-/genus-specific
62 comparative metabolomics analyses to guide functional biochemical studies. For instance,
63 comparative metabolomics within the Rhamnaceae revealed that only the Ziziphoid clade of this
64 family possesses a functional triterpenoid biosynthetic pathway, whereas the Rhamnoid clade
65 predominantly developed diversity in flavonoid glycosides (5). In a previous study, we
66 implemented a metabolomics-centered fragmentation rule-based pipeline to annotate the diversity
67 of 17-hydroxygeranyl linalool (17-HGL) diterpene glycosides within the Solanaceae family and
68 revealed intense chemotypic structural variations combined with a patchy distribution of this
69 compound class as it appeared restricted to the *Capsicum*, *Lycium* and *Nicotiana* genera (6). The
70 latter "phylometabolomics" information facilitated gene candidate selection for functional
71 biochemical studies in the 17-HGL diterpene glycoside pathway (6). Similarly, comparative
72 metabolomics across multiple Solanaceae species was instrumental in guiding co-expression
73 studies for gene discovery for the steroidal glycoalkaloid pathway emblematic of the *Solanum*
74 genus (7).

75 Besides inter-specific variations in SMs, another important dimension, unfortunately
76 rarely integrated into taxonomic-scale metabolomics studies, is the tissue/organ specialization of
77 most SM pathways. Exploring these tissue/organ-level variations and their statistical correlation
78 with gene expression data can be extremely powerful in the process of SM biosynthetic gene

79 discovery (8). Analyzing tissue-specific metabolomes is also critical to test ecological theories of
80 plant investments into metabolic defenses such as the optimal defense theory which predicts
81 greater metabolic defense accumulation in developmental stages/tissues with higher organismic-
82 level fitness contribution and/or greater predation rates (9). Trichomes, in particular glandular
83 ones covering most aerial plant tissues, are notorious for their capacity to synthesize high amounts
84 of very specific SMs (10). Trichome SMs can be either stored within trichome cells and glands or
85 actively secreted, such as for Solanaceae-specific poly-acylated sugars, also referred to as *O*-acyl
86 sugars and whose biochemistry has been thoroughly investigated in recent years (11). Calyces
87 formed by the floral sepals and which protect maturing reproductive organs are typically rich in
88 SMs whose biosynthesis can be dependent on trichomes present on these tissues (12–14). SM
89 profiles of roots, while much less systematically explored than shoot-based ones, can be as
90 structurally diverse as trichome-specific ones (15) and have recently become of major focus for
91 our understanding of SM ecological functions for plant-soil microorganisms' interactions (16).

92 Most recent advances in computational metabolomics provide a long-awaited framework
93 to systematically explore the above-described importance of the species \times tissue SM variations
94 (4). These novel capacities to explore plant chemical spaces are further propelled by platforms
95 such as, the MassIVE database (<https://massive.ucsd.edu/>) reaching 12000 metabolomics datasets
96 in 2022. Despite the increasing amount of data that can be generated from modern MS
97 instruments, the average annotation rate of most MS metabolomics studies remains at the order of
98 a few percent of deconvoluted MS/MS features (17). The number of computational tools to
99 address this challenge of transforming spectral information into chemical knowledge is hence
00 rapidly increasing and can be divided into two main approaches. One set of approaches relies on
01 MS/MS spectral grouping, as embodied by the game-changing development of molecular
02 networking and of the repertoire of network annotation/mining tools embedded within the GNPS
03 ecosystem (18, 19). A second set of approaches relies on *in silico* fragmentation and
04 (sub)structure prediction from mass spectra. Classification of spectra within ontologies of
05 molecular families can notably be achieved by CANOPUS, a deep neural network method which
06 is able to predict 2497 compound classes (20) and which is embedded with the elemental formula
07 prediction and structure annotation pipeline from SIRIUS (21). Alternatively, the MS2LDA
08 method allows to extract information derived from shared substructures from spectral data via a
09 Latent Dirichlet Allocation algorithm borrowed from topic modelling (22). Recently developed or
10 significantly upgraded computational tools such as CFM-ID (23), molDiscovery (24), Metfrag
11 (25) or QCxMS (26) provide algorithmic means to predict MS/MS spectra from structures.

12 However, systematically prioritizing and/or merging the highest confidence predictions from each
13 of these tools remains a challenge that is rarely tackled in most MS metabolomic studies.

14 The genus *Nicotiana* L. combines several appealing features to study SM pathway
15 diversification. This genus, comprising 13 well phylogenetically-resolved sections for a total of at
16 least 80 species, is appearing in various morphological forms such as small herbs to shrubs up to
17 small trees, which often are viscid-glandular and rarely glabrous (27, 28). Among the most
18 studied species in this genus are *Nicotiana tabacum* and *N. rustica*, which are traditionally grown
19 for tobacco products; *N. glauca*, which has been a focus of biofuel research studies (29) and *N.*
20 *benthamiana*, a very popular model organism in molecular biology (30). The intense research on
21 *Nicotiana* species is further reflected into the very large set of reference transcriptome and
22 genome resources publicly available for species of this genus (31). As recently reviewed (32), the
23 phytochemistry of several species of this genus, in particular that of the coyote tobacco *Nicotiana*
24 *attenuata*, a flagship model organism for the chemical ecology of plant-insect interactions (33),
25 has been extensively studied with notable focus on alkaloids, mono/sesquiterpene volatiles, O-
26 acyl sugars or 17-HGL diterpene glycosides. Finally, half of the species of the *Nicotiana* genus
27 are allopolyploids of different ages and for some of them, the closest extant diploid progenitors
28 have been mapped, thereby providing a phylogenetics framework to study allopolyploidy-
29 mediated contributions to phenotypic trait evolution (34). Among the *Nicotiana* SM innovations
30 thought to have been shaped by recent allopolyploidization events are *N*-acyl-nornicotines
31 (NANNs), derived from the *N*-acylation of nornicotine with long chain fatty acyl chains and
32 which have been described as specific to allopolyploid species of the section *Repandae* (35). This
33 *Nicotiana* section is about 4.5 million years old and has *N. sylvestris* as its closest diploid
34 maternal and *N. obtusifolia* as closest paternal progenitor. The 17 NANN structures originally
35 described in the *Repandae* species *N. repanda*, *N. nesophila*, *N. stocktonii* (36, 37), but not in *N.*
36 *nudicaulis*, likely act as gain-of-function anti-herbivory defenses. Indeed, compared with the
37 *Nicotiana* widespread nicotine and nornicotine non-acylated alkaloids, NANNs are highly
38 effective against and evade the resistance acquired for nicotine/nornicotine by the tobacco
39 hornworm *Manduca sexta*, a native herbivore (38). However, the evolution of this defensive trait
40 is largely underexplored and detailed investigations on the NANN structural diversity within the
41 genus *Nicotiana* are missing.

42 Here, we implemented a comprehensive computational MS metabolomics workflow to
43 explore SM chemodiversity in various tissues of 20 species representative of the main
44 phylogenetic sections within the *Nicotiana* genus. By employing a multi-inference deep
45 annotation approach that ultimately connects information theory statistics, chemical class

46 mapping and substructure inferences, we provide an unprecedented cartography of SM tissue-
47 level distribution in this genus. The results of this study provide access to novel SM annotations
48 and tissue x species distribution data to guide future biochemical studies and notably shed light on
49 the unsuspected structural diversity and evolutionary trajectory of the NANNs defensive pathway
50 within the *Nicotiana* genus.

51

52

53 **Results**

54 **Tissue-level metabolomics data capture phylogenetically-relevant *Nicotiana* SM diversity**

55 In order to comprehensively explore tissue-level SM diversification in the *Nicotiana* genus, we
56 profiled the metabolome of leaves elicited or not with methyljasmonate, concentrated leaf surface
57 exudates, complete root and of calyces (**Fig. 1B**) of 20 species covering all of the main sections of
58 this genus as well as diploid and allotetraploid states (**Fig. 1A** and **Table S1**). Besides
59 phylogenetic position, species selection further took into consideration the availability of
60 transcriptomics/genomics data as a platform for future functional studies (31). Sampled tissues
61 were selected based on previous studies of our group (8) indicating the high degree of tissue-level
62 specialization in SM distribution and conversely the importance of concatenating multi-tissue
63 profiles to increase SM coverage. Additionally, we aimed via this pluri-tissue approach to explore
64 tissue-level shifts in SM class prevalence across the focal species as a mechanism of organismic-
65 level chemodiversification. Noteworthy, amounts of leaf exudate material collected greatly
66 differed among the focal species, with *Nicotiana setchellii* (2.7 mg of exudate *per g* leaf fresh
67 weight) and *Nicotiana glutinosa* (2.5 mg/g) producing the largest amounts of dried exudates
68 collected from leaf washes (**Fig. S1** and **Table S1**). All methanolic extracts were analyzed using a
69 previously established UPLC-ESI⁺QTOFMS method with optimized settings for massive MS/MS
70 data collection (6). 17901 metabolite-derived MS/MS spectra (hereafter referred to as features)
71 were, after a data redundancy and contaminant check using a custom script, deconvoluted and
72 considered for Feature-based Molecular Networking (FBMN) processing with settings that were
73 optimized to handle the species \times tissue-exacerbated metabolic diversity in the dataset. The
74 resulting species \times tissue MS/MS feature compendium served as input for the data exploration
75 workflow presented in **Fig. 1D** (**Fig. S2**).

76 To contrast patterns of feature diversity across species, we calculated, for each of the
77 tissue types, α -diversity scores based on the Shannon Entropy (H) from Information Theory (8)
78 (**Fig. 2A**). A unifying trend in these tissue-level analyses was that species' profiles, differed
79 extremely in their α -diversity indices, up to 3-fold counter-species variations being detected
80 depending on the tissue type. Root samples were, from all examined plant samples, those with
81 consistently lower α -diversity scores (average $H = 7.6$), likely indicative of the prevalence of only
82 a few SM classes in these samples for the analytical conditions considered in this study (**Fig. 1C**).
83 As expected, highest α -diversity scores were on average detected for MeJA-elicited leaves
84 (average $H = 9.4$) (**Fig. S3**), followed by uninduced leaves (average $H = 9.3$) and calyces (average
85 $H = 9.0$). The effect of the MeJA elicitation on feature diversity was consistently more apparent at

86 the level of detected features and very variable among the focal species (**Fig. S3**). Interestingly,
87 we noted that these inter-species variations in MeJA inducibility (indicative of the amplitude of a
88 “metabolome plasticity” to this treatment) were strongly negatively correlated (Pearson
89 Correlation Coefficient = -0.76, P -value = 1.04×10^{-4}) with α -diversity scores of uninduced
90 leaves (“constitutive diversity”) (**Fig. S3**). Additionally, while we initially assumed that the
91 metabolic profiles of the exudates collected from uninduced leaves would be restricted to a few
92 prevalent SMs (thereby resulting in low α -diversity scores for this sample type), the
93 relatively high α -diversity scores detected in most species were consistent with a far greater
94 chemical diversity in those extracts. In clear contrast, *Repandae* species, with the exception of *N.*
95 *nudicaulis* and the hybrid *N. sylvestris* \times *N. repanda*, exhibited much lower α -diversity scores (H
96 ranging from 3.5 to 3.7 compared with the average H value of 8.5 for the rest of the species) that
97 were in line with the previously reported over-dominance of NANNs within their exudates (37).
98 When feasible based on the species sampling, we also compared the α -diversity scores of
99 allotetraploid species to those of closest diploid progenitors. Independently of the tissue type
00 considered, we did not observe evidence of clear metabolic additivity in allotetraploid species,
01 which would translate into higher α -diversity scores as compared to those of closest diploid
02 progenitors (**Fig. 2A**).

03 To analyze the relatedness of species’ metabolomes, we further computed inter-species
04 metabolic distances based the molecular networking information and used the resulting distance
05 matrices for constructing “phylometabolomics” trees. Several studies had previously attempted to
06 construct such “phylometabolomics” trees but from single-tissue metabolome data. Here, we
07 constructed trees both from the tissue-level (**Fig. S4**) and combined tissue data (**Fig. 2B**). The
08 resulting “all tissues” phylometabolomics tree captured patterns of metabolome-relatedness that
09 were frequently in accordance with the species’ tree section-level grouping and relatedness (**Fig.**
10 **2B**). Among other interesting insights, *Repandae* species’ metabolomes, with the exception of
11 that of *N. nudicaulis*, appeared much closely-related at the “all tissues” metabolome level to that
12 the *Sylvestres* section from which their maternal progenitor had been associated with, than to the
13 *Trigonophyllae* section (paternal progenitor section) (**Fig. 2B, Table S2**).

14

15 ***Creating a cartography of Nicotiana SM class diversification***

16 After highlighting counter-species chemodiversity variations, we then systematically
17 characterized onto which SM classes they mapped. In analogy to gene family inference and
18 survey across focal species as a first step in phylogenomics, we first employed the CANOPUS

19 tool for *ad hoc* systematic compound class and chemical ontology predictions. To combine
20 FBMN and CANOPUS information, we implemented a frequency-based molecular network-
21 based propagation of CANOPUS (NP-CANOPUS) predictions, resulting into class predictions for
22 86.5 % of the total features within the 1586 networks retrieved by FBMN. CANOPUS “super-
23 class” and “most specific class” intensity distributions integrating all tissue samples of given
24 species were encapsulated as treemaps and mapped onto the species tree to provide a bird’s eye
25 view on class expansions and shrinkages (**Fig. 3B**). For the sake of simplicity, only a few of the
26 main tendencies are reported below; close-up views on particular “metabolic tiles” and tissue-
27 specific treemaps are accessible in **Data S1**. Most clearly apparent was the highest proportion of
28 “lipids and lipid-like molecules” in all species, with a significant fraction of these lipids being, in
29 many species, contributed by the saccharolipid sub-class commonly referred to as *O*-acyl sugars
30 in the Solanaceae. Browsing these treemaps supported the presence of high amounts of predicted
31 diterpenes in *N. tabacum*, *N. sylvestris* and the cross between *N. repanda* x *N. sylvestris* – the
32 latter hybrid having been initially incorporated to test progenitor chemical trait dominance.
33 Among other trends, this analysis also pinpointed on *N. setchellii* exhibiting the most diverse and
34 abundant set of “phenylpropanoid derivatives” from predicted 3-*O*-methylated flavonoids
35 (connected to network #361), simple hydroxycinnamic acids (network #990), up to coumarin
36 glycosides (network #532). Noteworthy, the performance of CANOPUS predictions was
37 nonetheless hampered for SMs that contained substructures from independent biosynthetic
38 origins, thereby resulting into heterogeneous CANOPUS ontologies. For instance, the large
39 “amino acids and derivatives” tile within the *N. glauca* treemap was mostly associated with
40 network #468, but the features embedded in this network were manually curated as *N*-
41 hydroxycinnamoyl-spermidine conjugates which are commonly encountered in leaves of
42 Solanaceae species as antiherbivore defenses (39). Also highlighting this limitation was that the
43 high-level of NANNs which are emblematic of the *Repanda* section, was not as easily noticeable
44 on the corresponding treemaps. Previously characterized NANNs were indeed split into several
45 classes as “organoheterocyclic compounds”, “benzenoids” and “organic nitrogen compounds”
46 (**Data S1**).
47

48 ***Deep metabolome annotation empowered by a multi-inference approach incorporating a 1*** 49 ***million natural product in silico spectral database and consensus substructure computations***

50 The previous analysis indicated a critical need not only for broadly increasing feature annotations
51 beyond CANOPUS class predictions but also for gaining structural insights into core
52 (sub)structures underlying molecular networks’ topology. As outlined in a recent review (40),

53 substructure annotation provides information on functional groups, building blocks, or scaffolds
54 within a chemical structure. This level of information is complementary to compound class
55 prediction, most commonly addressing biosynthetic origin and/or compound physico-chemical
56 properties. To propel substructure identification in our dataset, we first optimized a multi-
57 inference annotation pipeline (**Fig. S2** and **S5**). Briefly, feature spectra were first queried against
58 an in-house *Nicotiana attenuata* SM MS/MS database (NaMS, entries resulting from the analysis
59 of purified SMs) and the GNPS library, the resulting hits being referred respectively to as
60 annotation levels 1 to 2 according to the Metabolomics Standard Initiative nomenclature (41).
61 Interrogation of these two experimental spectral databases provided hits for 4% of the MS/MS
62 features (**Fig. 3A**). Level 3 of the annotation nomenclature regrouped class-based annotations
63 mostly derived from manual inspection of network-level hits (5%). To circumvent limitations in
64 the chemical space covered by these two experimental databases, spectral interrogations were
65 conducted in parallel against *in silico*-predicted MS/MS spectral libraries using both
66 molDiscovery which predicts MS spectra of small molecules on-the-fly and scores their
67 probabilistic modeling (24), and a combination of CFM-ID and MatchMS. To further expand the
68 power of this approach beyond the chemical space of the molDiscovery built-in library, we
69 computed MS/MS spectra for the 429 natural products reported in a recent *Nicotiana*
70 phytochemistry review (32) and, more importantly, we undertook the development of an *in silico*
71 spectral library for about 1.1 million natural products (1M-NP).

72 A comprehensive description of the creation of the 1M-NP *in silico* spectral library and of
73 its architecture is reported as **Supplementary Text** (see also **Fig. S6 and S7**). The capacity of
74 such *in silico* spectra-based approach to increase the annotation coverage of plant SM profiles has
75 initially been exemplified in a pioneer study by Allard et al. (2016), but was restricted to chemical
76 entries (~ 220,000) retrieved from the copyrighted Dictionary of Natural Products
77 (<http://dnp.chemnetbase.com>). Here, we concatenated chemical structures derived from several
78 public natural product libraries (**Table S3**), which resulted, after filtering out duplicated InChI
79 representations and CFM-ID-based computation of composite MS/MS spectral predictions, into
80 1,066,512 unique MS/MS spectra that covered a vast proportion of the natural product chemical
81 classification proposed by NP-classifier (43). As CFM-ID version 4.0 computations returned
82 slightly different MS/MS spectra for stereoisomers – see MS/MS spectra predicted (+)-/(-)-
83 shikonin and (+)-/(-) thalidomide in **Fig. S8** –, stereoisomers were kept in the library. Altogether,
84 this important computational delivery of this study represents, to the best of our knowledge, the
85 largest natural product-derived *in silico* spectral library and is now available for spectral
86 interrogation as part of the GNPS ecosystem (**Data and Material Availability**).

87 The above-described multi-query approach of the 17901 features from our dataset
88 retrieved annotations for 57 % of these features, with 9 % hits for priority levels 1-to-3 (**Fig. 3A**).
89 To maximize structural insights that could be gained from this deep annotation, we finally
90 computed the top most common substructures (referred to as Network Consensus Structure, NCS)
91 based on feature annotations for each of the FBMN molecular networks that did not contain any
92 level 1-to-2 annotations. Consensus structure computational prediction relies on a new
93 algorithmic approach that employs hits obtained from *in silico* MS/MS spectral databases (See
94 description in the **Method section** and **Code Availability and Description**). The NCS strategy is
95 illustrated in **Fig. 3C-D** with top NCS hits for network #486 whose MS/MS features were initially
96 classified as “Amino acids and derivatives” by CANOPUS. A complete overview of the top NCS
97 predictions is summarized in **Data S3**. Altogether, this unique combination of different
98 computational approaches generated a multi-modal SM cartography that can be navigated from
99 CANOPUS-based ontology predictions down to sets of molecular networks connected to a given
00 class level and further down to predicted shared substructures within these networks (**Data S3**
01 and **S4**).

02

03 ***Exploring the chemical substructure basis of Nicotiana section and species-level SM***
04 ***specialization***

05 Next, we navigated the SM cartography to further dig into the inter-species chemodiversity
06 variations that were detected from the species-level α -diversity (**Fig. 2**) and CANOPUS treemap
07 analyses (**Fig. 3**). To rigorously infer statistical associations between species and particular
08 CANOPUS “super-class” / “most specific class” predictions, we employed non-metric
09 multidimensional scaling (NMDS). NMDS is a powerful ordination technique in information
10 visualization that is frequently employed in ecology to spatially represent interconnections among
11 species or communities based on a series of univariate descriptors (44). The strength of this
12 statistical approach is that it allows to efficiently collapse the information from multiple
13 dimensions (here summed peak areas and connected CANOPUS predictions) into a limited
14 number of descriptors exhibiting high-confidence statistical associations to species. Using
15 NMDS, we computed projections of species and CANOPUS predictions as intrinsic variables and
16 extracted strongest associations based on P -values < 0.05 (Permutation tests) and minimal cosine
17 scores for angular distances between these two set of entities in NMDS projections (**Fig. 4A**,
18 **Data S2**). A hierarchical clustering analysis of previously extracted most significant associations
19 resulted into four main clusters referred to as Family Clusters (FC) (**Fig. 4B**). Distribution of
20 these associations was not directly consistent with the species-/section phylogeny and thereby

21 indicative of gains and losses in species/section-level capacities for the abundant production of
22 specific SM core structures. Family Cluster 1 (FC1) regrouped predictions associated to *O*-acyl
23 glycerol structures that appeared to be prevalent within species of the section *Suaveolentes* and to
24 a lower extend in the *Petunoides*, *Polydicliae*, *Paniculatae* and *Rusticae*. In accordance with the
25 pronounced expansion of this compound class in the *Nicotiana* genus (11), *O*-acyl sugar
26 predictions enriched in FC2, exhibited widely distributed significant species associations
27 throughout the genus. Such associations were remarkably absent for the section *Repandae*, with
28 the exception of *N. nudicaulis*. Strong associations with predicted terpenoid structures caught our
29 attention when inspecting FC3. Most distinctive ones were detected for sections *Nicotiana* and
30 *Sylvestres* as well as for more distantly related sections *Undulatae* and *Tomentosae*. FC4 mostly
31 captured associations with phenylpropanoid-derived substructures and alkaloids, the latter further
32 emphasizing on the richness of alkaloid metabolism in the *Repandae* section.

33 A detailed interpretation of these species/section metabolic specificities requires a
34 simplified access to the underlying MS/MS fragmentation schemes. The latter can typically be
35 approached through MS2LDA, an unsupervised method to extract common patterns of mass
36 fragments and neutral losses, referred to as mass motifs, from collections of fragmentation spectra
37 (22). From this analysis, we retained 76 mass motifs that best depicted the structural diversity
38 within our dataset as confirmed by hierarchical clustering (resulting in clusters of co-varying mass
39 motifs) and mapping of enriched CANOPUS predictions for each mass motifs (motif-level
40 propagation of CANOPUS predictions) (**Fig. 5A**, **Fig. S9**). In analogy to the critical role of
41 conserved domain/motif inferences in protein structure-activity studies, mass motif inference
42 offers a dimensionality reduction perspective on recurrent fragmentation patterns derived from
43 particular substructures. This approach is however often limited by the scarcity of structurally
44 annotated mass motifs in MS2LDA libraries. An asset of our approach is that it mutualizes the
45 previously described SM cartography to mine most interesting mass motifs (**Fig. 5B** and **Data**
46 **S5**). For instance, we confirmed the presence in motif cluster 1 (MC1) of a mass motif
47 (*Strepsalini_110*) which was characteristic of the *O*-acyl glycerols specific to *Suaveolentes*. MC1
48 also contained motif #631 and motif #254 characteristic of steroidal glycoalkaloids and that were
49 strikingly specific to *N. plumbaginifolia*. Motif #646, present in the second cluster (MC2)
50 captured the complete diversity of 17-HGL diterpene glycosides, allowing to efficiently explore
51 tissue-specificity for this compound class. MC4 contained a motif (motif #37) with fragments
52 indicative of hydroxycinnamic acid substructures derived from a network of *O*-phenolic
53 glycosides. Similarly using inferences derived from these different computational approaches, we
54 could efficiently inspect motifs corresponding to previously mentioned *N*-hydroxycinnamoyl-

55 spermidine conjugates specific to *N. glauca* (MC5, motif #473), di- and triterpenoids abundantly
56 found in *N. tabacum* (MC5, e.g. motif #555, #euphorbia_350) and mono-, sesqui- and diterpenes
57 (MC5, motifs #558, #675 and #576 respectively) in sections *Nicotiana* and *Sylvestres* as well as
58 *Undulatae* (Fig. S10). As previously implemented for molecular networks (Fig. 3), mass motifs
59 can also be used for consensus substructure computations (Motif Consensus Structure, MCS), the
60 latter providing a further mean to circumvent the scarcity mass motif annotation in MS2LDA
61 libraries. All 76 MCS computations, combined with CANOPUS predictions and manual curation,
62 are presented in **Data S6**.

63

64 ***N-acylnornicotine (NANNs) as case-study for structural diversity expansion in Repandae***
65 ***allopolyploids***

66 In the following, we exemplify using the case-study of NANNs, how the *Nicotiana* genus SM
67 cartography and connected annotation resources can be exploited to gain novel (bio)chemical and
68 evolutionary insights into specific SMs. NANNs have been described as leaf exudate
69 allopolyploidy-mediated innovations specific to the *Repandae* section (35). In our data-platform,
70 NANNs' structural diversity was readily inferable from mass motif #433 (MC7) that included the
71 two main nornicotine substructure molecular fragments at *m/z* 132.0825 and at *m/z* 149.1075 (Fig.
72 6A). Inspection of this motif retrieved a far greater structural diversity than previously reported,
73 with 102 of annotated NANNs, not counting novel non-canonical NANN structures with three N
74 (NANNs integrating an aminated fatty acyl chain) or three O atoms (di-hydroxylated NANNs) or
75 those built on an anatabine scaffold instead of nornicotine (Data S8). This NANN structural
76 diversity directly translated from variations at the fatty acyl moiety level, with the presence of *iso*-
77 /*anteiso*-branched or straight C₁ to C₁₈ chains, with or without hydroxyl groups. As their structure
78 had not been unambiguously identified in previous phytochemical reports (35), the most abundant
79 hydroxy NANNs were purified and elucidated by NMR to confirm the unusual position of the
80 hydroxy group at position 3 (Fig. S11, Supplementary Text).

81 Total NANN pools were extremely high in leaf exudates and in trichome-rich calyces of
82 the *Repandae* species, but at barely detectable levels in *N. nudicaulis* (Fig. 6B). Most
83 surprisingly, our data mining revealed that roots harbored a previously unexplored diversity of
84 NANNs, albeit at almost 2 orders of magnitude lower than in leaves, and with very different
85 chemotypes (Fig. 6B). In this respect, cross-tissue comparisons of fatty acyl moieties among
86 NANN chemotypes indicated a general tendency towards shorter chain NANN (most notably C₈-
87 nornicotine and formyl-[C₁]-nornicotine) accumulation in root tissues (Fig. S12). A closer
88 inspection of previously noted non-canonical NANNs captured by this exploratory approach led

89 to the formulation of structural assignments for 4 structures harboring a second intra-chain
90 hydroxyl group, and 4 additional ones bearing a third N atom as part of an intra-chain amine
91 group (**Fig. 7A**). These non-canonical NANNs were purified; but due to insufficient yields, their
92 structure could not be further interpreted by NMR. In agreement with the presence of a third N
93 prone to be positively charged, these non-canonical NANNs mainly appeared in the form of their
94 $[M+2H]^{2+}$ and exhibited higher polarity than regular ones. Features corresponding to these non-
95 canonical NANNs shared with canonical ones the mass motif #433 associated with the
96 nornicotine backbone fragmentation, but were located in different molecular networks (**Fig. 7A**)
97 that were specific to the *Repandae* section (**Fig. S13**). These *Repandae* non-canonical NANNs
98 were further analyzed by ultra-high resolution MALDI MS imaging experiments conducted from
99 leaf cross-sections of *N. nesophila*. These analyses supported their uniform distribution within the
00 leaf lamina, the corresponding MSI images overlapping with those of well-known lamina-
01 distributed SMs such as chlorogenic acid, and not specifically on the leaf surfaces as for canonical
02 NANNs (**Fig. 7B**, **Fig. S14**).

03

04 ***NANNs evolutionary diversification predates Repandae polyploidy formation***

05 Our data strongly challenged the previous view that NANN biosynthetic capacity strictly arose as
06 part of the allopolyploidy event at the base of the *Repandae* and that as such NANNs could be
07 considered as a transgressive metabolic trait to this section. Indeed, **Fig. 6** shows that the
08 NANNs' diversity pervades the different *Nicotiana* sections, albeit at extremely low levels in all
09 the species examined additionally to the *Repandae* section. Obviously, complete leaf extracts of
10 *N. nesophila* ($H=3.25$, 53 NANNs) and *N. repanda* ($H=3.17$, 49 NANNs) exhibited the overall
11 greatest NANN α -diversity values (**Fig. S15**). Of all leaf exudate samples examined, the NANN
12 α -diversity calculated for hybrid *N. repanda X sylvestris* ($H=3.03$, 18 NANNs) was the highest,
13 which reflected a balanced distribution among NANN relative intensities in this sample. By clear
14 contrast, lowest NANN α -diversity values were detected for leaf exudates of *N. repanda* ($H=0.42$,
15 24 NANNs), *N. stocktonii* ($H=0.39$, 22 NANNs) and *N. nesophila* ($H=0.54$, 24 NANNs), which
16 further indicated, besides the high NANN biosynthetic capacity in these species, their exacerbated
17 specialization towards C₁₄-OH-nornicotine exudation. In this respect, while the NANN
18 chemotypes of the leaf exudates of almost all of the focal species were characterized by the
19 dominance of this particular NANN, *N. rustica* and *N. setchellii* were noticeable exceptions, being
20 dominated by C₁₆-nornicotine (**Fig. 6C**) and *N. glutinosa* for its exclusive accumulation of
21 formyl-nornicotine. As previously noted (**Fig. 6B**), roots of almost all species harbored a rich
22 diversity of NANN, particularly exacerbated in *N. obtusifolia* ($H=2.26$, 8 NANNs), predicted as

23 one of the closest diploid progenitors to the *Repandae* section. Altogether, a most parsimonious
24 explanation to the evolution of the NANN pathway was that it predates *Repandae* formation.
25 Such an evolutionary scenario appeared to be supported in all tissue-level ancestral state
26 reconstruction (ASR) analyses carried out based on a *matK*-based species tree and with total
27 NANN levels expressed as discrete states (Fig. 8). The ASR analysis computed from total root
28 NANNs in combination with tissue-level NANN chemotypes, further suggested that the last
29 common ancestor to the examined species had a consequent root-based NANN accumulation
30 capacity.

31

32 Discussion

33 Lineage-specific reconfigurations in rapidly evolving sectors of a plant specialized metabolism
34 can be transparent at the genomics/transcriptomics levels for which most evolutionary studies on
35 adaptative traits are conducted. This stresses the obvious fact that the power of genomics-driven
36 evolutionary inferences on plant SM pathways critically relies on the chemical classification of
37 metabolites part of these metabolic sectors as well as on the phylogenetics contextualization of
38 this information. To tackle this issue, the open-source computational metabolomics approaches
39 presented here are propelled by a broadly transposable multi-inference annotation that maximizes
40 the coverage of substructure predictions, thereby resulting into an unprecedented cartography of
41 SM diversity in the *Nicotiana* genus linking species-level SM prevalence to particular
42 substructures. With this workflow, we notably shed light on the structural diversity and
43 phylogenetics distribution of NANNs, a gain-of-function defensive innovation previously thought
44 to have evolved with *Repandae* allopolyploids speciation (38).

45 A major challenge in MS metabolomics remains to reach broad structural annotation
46 (“deep metabolome annotation”) and substructure discovery beyond chemical class predictions
47 and the dereplication of previously identified SMs, which is the most frequent outcome of
48 molecular networking-based data exploration. In particular, with the use of heterogeneous
49 computational annotation tools and that of querying highly diverse experimental and *in silico*
50 MS/MS database comes the inherent difficulty of systemically prioritizing and/or merging the
51 minimal set of most reliable annotations collected from these inferences. MolNetEnhancer has
52 been developed to more efficiently combine outputs from molecular networking, MS2LDA as
53 well as *in silico* and chemical classification tools (45). However, substructure discovery from
54 MolNetEnhancer outputs is strongly hampered by the scarcity of annotated motifs in the
55 Mass2Motifs database embedded into MS2LDA, many of which additionally translating from
56 relatively unspecific fragmentations (e.g. water, methyl, hexose losses). Only 24 of the 76 mass

57 motifs retained for further analysis had partial annotation hints in the MS2LDA Mass2Motifs
58 database (**Data S5**). To significantly improve substructure discovery and annotation, we
59 implemented two complementary approaches. On the one hand, we propagated CANOPUS
60 predictions at mass motif level (MP-CANOPUS) by computing frequencies in “super-class/sub-
61 class/most specific class”, and combined this information with mass motif co-regulation analysis
62 (**Fig. 5**). The second approach implemented for substructure analysis involved advanced
63 maximum common substructure calculations to integrate annotations from multiple tools on a
64 network (NCS) or motif level (MCS). Overall, we obtained 349 NCS or 303 MCS predictions for
65 the whole data-set (**Data S3 and S6**). Maximum common substructure computation for
66 substructure prediction had been employed in one of our previous studies to cluster candidate
67 structures obtained by the MetFrag searches among co-regulated herbivory-induced metabolites
68 (46) and is also one of the processing steps within the Network Annotation Propagation tool of
69 the GNPS web-platform (47). Altogether, we advocate that the NCS/MCS approach implemented
70 here has three main advantages: *(i)* it is an efficient mean of summarizing common substructure
71 within the diversity of outputs from database queries as SMILES strings, *(ii)* it can be used as input
72 to reveal substructures statistically associated with intense chemodiversification in a given
73 species, and *(iii)* it provides structural guidance during the manual interpretation of mass motifs or
74 molecular network. In this respect, our study led to the curation of 76 mass motifs (**Data S5**).
75 Such effort is important to empower supervised search of mass motifs which is already possible in
76 MS2LDA and which will be greatly facilitated with the recent release of the MS2QUERY tool
77 (48).

78 A very important delivery of our work is the development and public sharing of the 1M-
79 DB which is, to the best of our knowledge, the largest *in silico* spectral database. This approach
80 resulted into 5-fold more hits (annotation of 57% of the total features), than experimental spectral
81 database interrogation alone. Data of the 1M-DB can currently be accessed and interrogated from
82 the GNPS platform. The size of this data-set can represent a challenge for MatchMS-based
83 queries, which can nonetheless be locally implemented with reasonable computing capacity with
84 the parallelized script (**Code Availability and Description**) provided with our study. It is
85 therefore foreseeable that the efficiency of the interrogation of the 1M-DB will strongly benefit
86 from up-to-date optimization of MatchMS parallelization as part of future version releases.
87 Multiple tools have been developed in recent years to produce hypothetical MS/MS spectra (23–
88 26, 49). A more recent development in this area is that of QCxMS which provides, in our
89 experience, very high-quality spectra. This program is currently too much computationally
90 demanding and could not be transposed to the scale of this study, besides the computation of

91 MS/MS predictions for the 429 structures of the Jassbi database and using a limited number of
92 fragmentation trajectories (Zenodo link, <https://doi.org/10.5281/zenodo.6536010>). One promising
93 direction for improving the confidence of such *in silico* fragmentation-based annotation is
94 exemplified by the recently developed COSMIC workflow that incorporates a confidence score
95 consisting of kernel density *P*-value estimation from a decoy library and a support vector machine
96 algorithm (50). With the increasing quality of MS/MS predictions, one interesting perspective
97 could be to extract mass motifs from them and thus directly infer fragment substructures produced
98 from known structure *in silico* decomposition.

99 In terms of structural information, the SM metabolic cartography generated in this study
00 goes far beyond to a recently published chemotypic classification of the *Nicotiana* genus which
01 mostly consisted in the dereplication of primary metabolites such as steroids and only a few SMs
02 (51). In our opinion, this data platform and our SM cartography provide complementary views on
03 the metabolic diversity of this genus. Noteworthy, the aforementioned study did solely focus on
04 leaf metabolomes, while ours and previous studies (8) unambiguously indicated the importance of
05 “screening” multiple tissues to capture a broader SM diversity picture. In this respect, we
06 demonstrated that expanding the analysis at the multi-tissue level (by combining tissue-level
07 molecular network information) resulted into a “phylometabolomics” tree that captured shared
08 SM biosynthetic potential among closely-related species with more resolution (**Fig. 2**). Beyond
09 simple presence/absence of SM classes which has been a traditional focus of chemotaxonomic
10 studies, the fact that structural diversity can nowadays be more efficiently accessed with
11 computational MS metabolomics opens novel research avenues for understanding the evolution of
12 SM, as implemented in a recent survey of the SM synapomorphies and homoplasies in the
13 Malpighiaceae family (52). Information theory Shannon statistics transposed to MS feature
14 analysis or individual metabolites can also provide an efficient means of contrasting metabolic
15 diversity among the metabolic profiles to examine evolutionary ecology theories and
16 contextualize those at relevant taxonomic scales (53). By employing α -diversity analysis, we
17 confirmed that roots exhibit, under our analytical conditions, the most specific metabolomes, a
18 pattern which had been previously detected in a study focusing on *N. attenuata* as the sole model
19 species (8). α -Diversity scores further varied in-between species, thereby indicating variations in
20 constitutive SM biosynthetic capacities and/or constitutive vs stress-induced investments into SM
21 production. In this respect, we further observed that these inter-species variations in MeJA
22 inducibility were negatively correlated with α -diversity scores constitutive leaf metabolome. This
23 trend is reminiscent of the inter-species patterns detected from the comparative analysis of early

24 herbivory-induced transcriptomes for 6 *Nicotiana* species (54), and may reflect physiological
25 trade-offs between constitutive vs inducible metabolic diversity maintenance.

26 Many interesting novel biochemical insights worth to be pursuing by gene function
27 studies, were extracted from the SM cartography produced from this study. Our analysis notably
28 detected the presence of mono-*O*-acylglycerols (classified under the CANOPUS most specific
29 class 1-monoacylglycerols) specifically on the leaf surfaces of the section *Suaveolentes* and at
30 lower abundances in the *Rusticae*. Besides its well-known housekeeping function in the synthesis
31 of di- and tri-*O*-acylglycerols via the action of GPAT enzymes (55), the latter compound class has
32 been poorly investigated regarding its presence on plant aerial surfaces. Main reports on the
33 possible defense-related functions of this compound class derive from studies on their presence as
34 abundant surface metabolites on the calyx of several Scrophulariaceae species (56), and from a
35 unique report for the *Nicotiana* genus describing these compounds as efficient chemical glues
36 against small insects on the leaf surfaces of *N. benthamiana* (57). The prevalence of this
37 compound class in the *Suaveolentes* section, in particular in *N. benthamiana*, along with the here-
38 described high levels of *O*-acyl glucoses (58) could point to an interesting case-study to
39 functionally examine the biochemistry and evolution of this pathway and compare it with that of
40 the thoroughly investigated and structurally reminiscent *O*-acyl sugars (11). Our analysis also
41 revealed subtle tissue-level chemotypic variations within *O*-acyl sugars networks. Apart fro,
42 confirming previously detected strong cross-species variations in structural diversity, inspections
43 of these networks also pinpointed that some of these *O*-acylsugars are present at low levels in
44 roots (Fig. S10). This could further illuminate recent work on the predicted role of these SMs in
45 plant-soil microbiome interactions (15). Our SM cartography also provided a far greater species \times
46 tissue resolution on terpene-related classes' distribution compared to tendencies previously
47 sketched in *Nicotiana* studies that targeted trichome-based cembrene diterpene (59) and 17-HGL-
48 DTG (6). Our study revealed for these two classes of diterpenes, pronounced expansions of
49 structural diversity and significant associations with the *Nicotiana*, *Sylvestres*, *Undulatae*,
50 *Tomentosae*, *Trigonophyllae* (17-HGL-DTG) sections that include species in which emblematic
51 structures of these compound classes had been originally detected (6). An unexpected result was
52 the detection, at large levels in *N. plumbaginifolia* and to a minor extent in *N. glutinosa*, of
53 steroidal glycoalkaloids, emblematic of the *Solanum* genus and whose presence is considered as
54 erratic in other Solanaceae genera. Within the structurally rich network of steroidal glycoalkaloids
55 identified in our study, the dereplication of solaplumbin m/z 722.4479, ($[M+H]^+$, $C_{39}H_{64}NO_{11}$) is
56 supported by old phytochemistry reports (60). Such unexplored patchy distribution of steroidal

57 glycoalkaloids within the Solanaceae provides exciting foundations for future evolutionary
58 biochemistry studies.

59 The fact that α -diversity scores, independently of the tissue type, were not reflecting direct
60 metabolic additivity in allotetraploid species. This, along with unique metabolic characteristics as
61 compared to their closest extent diploid progenitors, could be reminiscent of patterns observed
62 when inspecting complex reconfigurations of floral morphological and associated metabolic traits
63 in *Nicotiana* allotetraploids (34). Due to their previously reported absence in *Repandae* closest
64 diploid progenitors (*Nicotiana sylvestris* and *Nicotiana obtusifolia*), NANNs have often been
65 considered as “transgressive” metabolic traits derived from the *Repandae* allopolyploidization. In
66 our study, we annotated 102 NANNs, including 6 first elucidation by NMR, and discovered
67 NANN-related structures built from anatabine as a backbone, and the presence of novel NANNs
68 leaf lamina-based restricted to *Repandae* and incorporated uncommon aminated fatty acyl
69 moieties. Above all, our study indicates that the NANN biosynthetic capacity predates the
70 *Repandae* section formation. However, a main innovation of *Repandae* species is their capacity to
71 accumulate very high level of canonical NANNs on their surfaces as well as N₃-containing
72 NANNs in their leaf laminae. These data provide rigorous support to old literature that reports
73 anecdotal evidence (61, 62) for low amounts of short (-formyl, -acetyl) and middle (C₄-C₈) chain
74 length NANNs present in other *Nicotiana* species (63). Interestingly, *N. obtusifolia*, considered as
75 a closest extant female progenitor to *Repandae*, is one of the *Nicotiana* species that accumulates
76 the largest nornicotine-to-nicotine ratio in its leaves (64). Another interesting observation to
77 pursue is that *N. sylvestris*, the closest extant male progenitor to *Repandae*, is thought to have
78 contributed to several allopolyploidization events in the genus *Nicotiana*, many of which being
79 able to accumulate greater NANN amounts than the other species tested in this study. As such,
80 our data suggest a more complex than previously thought evolution of the NANN pathway. A
81 direct perspective will be the identification of the canonical NANN biosynthetic N-
82 acyltransferase(s) which is predicted to be abundant in *Repandae* trichomes from our data and
83 from previous phytochemical analyses on crude trichome fractions (35–37, 65). Our tissue
84 cartography finally revealed a largely unexplored repertoire of NANNs in the roots of all
85 examined species. These data and ASR analyses are in favor of shorter chain NANN production
86 in roots being a most ancestral trait in this metabolic class. In the context of future biochemical
87 investigations, the latter interpretation would be consistent with the fact that the accumulation of
88 canonical NANNs onto aerial surfaces involves trichome-based N-acyltransferase enzymes with
89 greater affinity for long chain fatty acyl-CoA as compared to those present in roots.

90 In conclusion, the fully open data and broad range of data integration approaches and
91 provided here present an unprecedented resource to revive SM analysis in the *Nicotiana* genus
92 and contribute to the establishment of phylometabolomics as an instrumental bottom-up approach
93 to guide future evolutionary biochemistry studies.

94

95 **Material and Methods**

96 ***Plant material, growth conditions and treatment***

97 *Nicotiana* species with their origin and associated accession numbers are summarized in **Table**
98 **S1**. Seeds of all *Nicotiana* species were directly germinated on soil, with the exception of *N.*
99 *attenuata*, for which smoke-induced seed germination was established as described previously
00 (Krügel et al., 2002). For all species, glasshouse growth conditions were as described previously
01 (Krügel et al., 2002). Six-to-eight weeks old elongated plants were used for all metabolomics
02 analyses. In order to analyze the regulatory function of jasmonate signaling on metabolomics-
03 inferred specialized metabolism classes, petioles of 2 elongated plants were treated with either 20
04 µL lanolin paste containing 150 µg methyl jasmonate (Lan + MeJA) or with 20 µL pure lanolin
05 (Lan) according to Heiling et al. (2021). Leaf samples were harvested 72 h after treatment, flash-
06 frozen in liquid nitrogen, and stored at -80°C until use.

07

08 ***Metabolite extraction procedures for UPLC-QTOF MS***

09 Leaf, root and calyx metabolites were extracted for UPLC-QTOF MS analysis as previously
10 described (Heiling et al., 2017). Briefly, for leaf samples, 12 discs *per* plant (~ 100 mg fresh-
11 weight tissue) were flash-frozen in liquid nitrogen immediately after harvest and stored at -80°C
12 until use. The latter frozen leaf samples were ground in a Tissue Lyzer II for 3 min at 30 Hz and
13 metabolites extracted by addition of 1 mL of 80 % methanol, 1 h of shaking at 1000 rpm at 4°C
14 and further kept with a gentle agitation overnight at 4°C. Samples were finally centrifuged for 10
15 min at 14000 g and the resulting supernatants transferred into glass vials. Root samples referred to
16 the complete root system of about-8 weeks old plants. After soil removal, roots were rinsed in
17 water, gently dried with paper towels and flash-frozen in liquid nitrogen. Root samples were
18 homogenized in a Tissue Lyzer II for 4 min at 30 Hz. Metabolite extraction was conducted as
19 above described from 200 to 400 mg root material (primary, secondary and tertiary roots). Flower
20 calyces were collected from about 8 weeks old plants and processed for metabolite extraction
21 using above leaf metabolite extraction conditions. To obtain leaf exudates enriched into semi-
22 polar to apolar surface metabolites, fully elongated leaves were briefly rinsed with acetonitrile.
23 These exudates were filtered on filter paper and completely dried under reduced pressure. Dried

24 residues were then re-dissolved in methanol and total metabolite concentration was adjusted to 1
25 mg.mL⁻¹, except for *Nicotiana repanda*, *N. stocktonii* and *N. nesophila* exudates which were
26 diluted to 0.001 mg.mL⁻¹ and 0.1 mg.mL⁻¹ (see **Table S1**) in order to avoid detector saturation,
27 due to the high levels of NANNs in these samples. Peaks areas were corrected by corresponding
28 dilution factors.

29

30 ***UPLC-QTOF MS chromatographic conditions***

31 Methanolic extracts were analyzed using ultra-high pressure liquid chromatography coupled to
32 high-resolution mass spectrometry on an UltiMate 3000 system (Thermo) coupled to an Impact II
33 (Bruker) quadrupole time-of-flight (QTOF) spectrometer. Chromatographic separation was
34 performed on an Acquity UPLC ® BEH C18 column (2.1x100mm, 1.7µm, Waters) equipped
35 with an Acquity UPLC ® BEH C18 pre-column (2.1x5mm, 1.7µm, Waters) and using a gradient
36 of solvents A (water, 0.1% acetonitrile, 0.05% formic acid) and B (acetonitrile, 0.05% formic
37 acid). Chromatography was carried out at 35°C with a flux of 0.4 mL.min⁻¹, starting with 10% B
38 for 3 min, and reaching successively 20% B at 12 min, 35% B at 17 min, 40% B at 23 min, 45%
39 B at 25 min, 50% B at 30 min, and 95% B at 40 min, holding 95% for 5 min and coming back to
40 the initial condition of 10 % B in 3 min. These chromatographic conditions (total running time of
41 48 min) were previously optimized for the comparative metabolomics of methanolic extracts of
42 Solanaceae species in one of our previous studies (Heiling et al., 2016). Samples were kept at 4°C
43 during the sequence of injections and 5µL per sample were injected in full-loop mode with a
44 washing step after sample injection involving 150µL of the wash solution (water:methanol, 80:20,
45 v:v).

46

47 ***Conditions for DDA MS/MS data collection during UPLC-QTOF MS analysis***

48 The Impact II QTOF instrument was equipped with an electrospray ionization source and
49 operated in positive ionization mode on a 50-to-1500 Da mass range with a spectra rate of 5 Hz
50 and by further using the AutoMS/MS fragmentation mode. The end plate offset was set at 500 V,
51 capillary voltage at 4500 V, nebulizer at 2 Bar, dry gas at 10 L.min⁻¹ and dry temperature at
52 200°C. The transfer time was set at 60-70 µs and MS/MS collision energy at 80-120% with a
53 timing of 50-50% for both parameters. The MS/MS cycle time was set to 2 seconds, absolute
54 threshold to 31 cts and active exclusion was used with an exclusion threshold at 3 spectra, release
55 after 1 min and an ion was reconsidered as precursor for the fragmentation if the ratio current
56 intensity/previous intensity was higher than 5. MS/MS collision energy was set according to the
57 mass from 25 V for a mass of 100 Da to 50V for a mass of 1 500 Da. The MS/MS spectra

58 acquisition rate was further optimized, from 3 Hz to 7 Hz, according to the intensity of the
59 observed mass. A calibration segment was included at the beginning of the runs allowing the
60 injection of a calibration solution from 0.05 to 0.25 min. The calibration solution used was a fresh
61 mix of 50 mL isopropanol:water (50:50, v:v), 500 μ L NaOH 1M, 75 μ L acetic acid and 25 μ L
62 formic acid. The spectrometer was calibrated on the $[M+H]^+$ form of reference ions (57 masses
63 from *m/z* 22.9892 to *m/z* 990.9196) in high precision calibration mode with a standard deviation
64 below 1 ppm before injections, and re-calibration of each raw data was performed after injection
65 using the calibration segment.

66

67 ***Ultra-high resolution MS imaging data acquisition and processing***

68 Freshly collected rosette leaves of *N. nesophila* were embedded into M-1 embedding matrix
69 (Thermo Scientific) and frozen before cutting. Cuts were done on a transverse plane at 25 μ m
70 thickness and -15°C using a cryotome FSE. Sections were deposited on indium-tin-oxide coated
71 slides and sprayed with a-cyano-4-hydroxycinnamic acid (HCCA) matrix at 10mg/mL in 70%
72 ACN, 0.1% trifluoroacetic acid using the HTX M5 sprayer. Nozzle temperature was set at 75°C,
73 flow rate at 0.120mL/min, velocity at 1200 mm/min, pressure at 10 psi, gas flow rate at 3 L/min
74 and nozzle height at 40mm. Four passes were applied with a track spacing of 3mm and a HH
75 pattern.

76 Samples were analyzed with a Burker SolariX 7T Fourier transform ion cyclotron mass
77 spectrometer at resolving power R=120,000 at *m/z* = 400. Acquisition was performed in positive
78 ion mode on a 100-500 *m/z* mass range, with an accumulation of 0.020 s, the transfer optics time
79 of flight set at 0.600 ms, frequency at 6 Hz and RF amplitude at 350 Vpp. The MALDI plate
80 offset was set at 100 V, deflector plate at 200 V, laser power was set at 20%, laser shots at 100
81 and frequency at 1000 Hz with a small laser focus. The instrument was calibrated by multipoint
82 correction using the peaks of the HCCA matrix (*m/z* = 379.0924, 399.0377, 401.0744, 417.0483).
83 The regions of interest were determined in FlexImaging with a raster width of 50 μ m. Images of
84 the ions of interest +/- 3 ppm were displayed in MSiReader v1.03 (66). The data was submitted to
85 metaspace and is available at https://metaspace2020.eu/project/nicotiana_msi-2022

86

87 ***Feature-based molecular networking of UPLC-QTOF MS data***

88 Raw data were converted to the .mzML format using MSConvert (Version 3.0.21112-b41ef0ad4,
89 Chambers et al., 2012). The resulting data files were then processed with the Batch Mode (See
90 Code availability, Script S10) of MZMine 2.53 (68) and exported for Feature-based molecular
91 networking (FBMN) analysis in the GNPS environment (Nothias et al., 2020; Wang et al., 2016)

92 and for spectral analyses in Sirius (21). The resulting .mgf and .csv files were further filtered to
93 exclude redundant none-biologically informative MS/MS features using newly developed Python
94 Scripts **S11** and **S12** (see Code availability). The m/z signals that appear more than 5 times (\pm
95 3ppm) with a retention time coefficient of variation greater than 10 % were discarded. This
96 filtering step excluded 11580 features (out of a total of 29481 retrieved from the MZMine-based
97 processing), a vast majority of those corresponded to redundant features detected at high-level in
98 solvent blanks. Finally, FBMN was performed using the modified cosine as spectral similarity
99 metric and with standard settings (Version release_28.2, except lower precursor and fragment
00 tolerance of 0.005 Da). Output of the FBMN analysis is available on GNPS at the following link:
01 <https://gnps.ucsd.edu/ProteoSAFe/status.jsp?task=cf822b6c7c914206941bb0b6007e7eb0>
02

03 ***MS/MS elemental formula and compound class predictions with Sirius***

04 Sirius (Version 4.8.2) was used to predict elemental formulas for MS/MS precursors as well as for
05 the deep neural network-based compound class prediction as part of the CANOPUS pipeline (20).
06 Sirius commands are summarized as part of Script **S13** (see Code availability). Elemental
07 formulas by Sirius were further processed with Scripts **S14** and **S15** (see Code availability) to
08 restore Feature IDs and calculate the degree of unsaturation of these formulas. A main strength of
09 CANOPUS-based class prediction is that does not involve the interrogations of spectral libraries
10 with fragmentation spectra, thereby allowing class prediction of MS/MS features for which no
11 database hit is retrieved and circumventing the possible issue of error propagation when false
12 class prediction is obtained by FBMN network-level propagation from feature-derived database
13 hits. MS/MS feature-level ontologies were retrieved from CANOPUS predictions as well as
14 FBMN network-propagated superclass, subclass and most specific class ontologies. The latter
15 ontology propagation was implemented using Script **S19**.
16

17 ***Mass motif inference by MS2LDA***

18 Mass motifs were inferred using standard settings of MS2LDA (Version release_23.1, Wandy et
19 al., 2018), submitted through the GNPS workflow. Available at:
20 <https://gnps.ucsd.edu/ProteoSAFe/status.jsp?task=6f325f462e1145bfb465c679c2ee17d6>
21 A total of 609 motifs were assigned including already existing motifs from motifdb. To explore
22 mass motifs assignments on a species level, a binary mass motif matrix for all tissues was created
23 by setting features above peak area of 10.000 to the value of 1 and those below to 0 (Script **S17**).
24 The resulting matrix was combined and presence was summed *per* tissue and then set again into a
25 binary matrix. Following this binary transposition of motif distributions, feature presence *per*

26 motif was determined *per* species, resulting in a motif count table (Script **S18**). This set of mass
27 motif counts (after filtering and manual curation 76 motifs), was then normalized by motif id and
28 clustered by hierarchical clustering using the Ward clustering method implemented in
29 MetaboAnalyst (69).

30

31 ***MS/MS annotation based on spectral database interrogations***

32 We implemented a 3-pronged approach to annotate MS/MS from the interrogation of
33 experimental and *in silico* fragmentation databases, similar as proposed in Sumner et al., 2007.
34 Level 1 in our priority assignment of annotations corresponded to hits retrieved from
35 experimental spectral databases and or NMR structural confirmation. Highest priority within level
36 1 of annotated spectra (level 1a) was given to hits confirmed by NMR in this work. Level 1b
37 annotations correspond to hits from spectral alignments (and correspondence of precursor *m/z*
38 values) using a local MatchMS (score above 0.65 and more than 6 matching peaks)
39 implementation (Script **S8**, see **Code availability**) with the modified cosine score, from an in
40 house high-resolution experimental MS/MS spectra database of *Nicotiana attenuata* specialized
41 metabolites and/or manual inspection of spectra. Level 2 corresponded in our annotation approach
42 to hits retrieved, with the cosine score from high-resolution MS/MS spectra of the GNPS
43 database. Level 3 annotations were considered for hits from alignments with *in silico* MS/MS
44 spectra or in the case of network propagation of hits from the experimental databases, both after
45 manual inspection. Jobs for the recently developed molDiscovery approach (Version 1.0.0, Cao et
46 al., 2021) were submitted through GNPS with both the molDiscovery built-in library and the
47 Jassbi compound database created as part of this study. The Jassbi compound database (429
48 structures) was compiled from structures extracted from a recent *Nicotiana* phytochemistry
49 review (32). *In silico* MS/MS spectra for the Jassbi compound database were also produced with
50 the fragmentation tool CFM-predict 4.0 (23) (Script **S5**, see **Code availability**) database
51 searching was performed with MatchMS (70) (Script **S9**).
52

53 ***Consensus substructure and molecular network chemical classes***

54 We implemented a new algorithmic approach to deal with the high number of annotations
55 retrieved from the various *in silico* MS/MS spectral databases. To this end, we used annotations
56 retrieved from Sirius (confidence score above 0.65), 1M-DB searched with modified cosine
57 (score above 0.5 and 5 matching peaks), CFM-DB 1M searched with spec2vec (score above 0.5),
58 Jassbi-CFM (score above 0.5 and 5 matching peaks) and Jassbi-molDiscovery. These annotations

59 were retrieved at the molecular network or at the MS2LDA mass motif level in order to calculate
60 consensus substructures for a given network (NCS) or mass motif (MCS).

61 Main steps involved in consensus substructure calculations involved the following commands
62 (Script **S16**, **S19**, see **Code Availability and Description**): (1) *fragment structures*, (2) *get the*
63 *most common fragments*, (3) *select the top 50 and only keep the ones with more than 12 atoms*,
64 *(4) cluster by structural similarity*, (5) *sort by cluster size*, (6) *calculate the maximum common*
65 *substructure within the cluster*, (7) *retrieve the top 4 results*.

66 To harness the vast amount of structural information classified by molecular networking,
67 we selected the top 252 networks sorted by only picking networks containing more than 10 nodes.
68 The peak areas within these networks were summed with Script **S24**. Peak areas were normalized
69 (Excel's STANDARDIZE function) by cluster id and the maximum on tissue level per species
70 was kept. The propagated CANOPUS classes were grouped their peak areas summed (Script **S28**)
71 and the resulting data was used to create per species treemaps in Excel. A summary of the Top252
72 molecular networks, their calculated consensus substructures and their propagated CANOPUS
73 classes can be found in **Data S3**. Additionally, **Data S4** and **S7** allow to navigate this multi-level
74 information at mass motif and network levels.

75

76 **Computing MS/MS-informed phylometabolomics species trees**

77 To create MS/MS similarity-based species, referred to in the text as phylometabolomic trees, we
78 used the data compiled as mentioned above (Script **S24**) (**Fig. 2A**) or the data from the motif
79 count (Script **S18**) (**Fig. S9**) in order to calculate the Euclidean pairwise distances between
80 species' metabolomes (Script **S20**). The resulting matrix was then used to plot trees in R with the
81 APE package using the Neighbor-Joining algorithm and bootstrapping 999 with iterations. (Script
82 **S21**)

83

84 **Ancestral state reconstruction for the relative occurrence of N-acylnornicotines**

85 We adapted the concept of ancestral state reconstruction (ASR) classically employed for the
86 evolutionary analysis of quantitative phenotypic traits for the exploration of NANNs' relative
87 occurrence. To this end, we first constructed a phylogenetic tree of the focal *Nicotiana* species
88 based sequences of the *matK* gene obtained from a previous study (71), the sequence of *N.*
89 *maritima* was used to account for *N. wuttkei* position within the species tree due to unavailable
90 genome data for the latter species. Laskowska and Berbec (2003) previously suggested the very
91 close relationship between the latter two species as well as reported their successful hybridization
92 in the wild. *Nicotiana setchelli* *matK* gene sequence was obtained from the assembly of

93 transcriptomics data publicly available for NCBI SRA accession SRR2106530. The species tree
94 was constructed using NGPhylogeny.fr (73) with default one click options and the PhyML
95 Maximum Likelihood method. For ASR, feature intensities accounting for the species and tissue-
96 wide NANN diversity were retrieved using the above-described mass motif characterization
97 approach. ASR was performed with the MBASR package (Heritage, 2021; Script **S25**) on peak
98 areas of the root that have been transformed into a ordered trait of 5 categories (**Fig. 8, Fig. S1**).
99

00 ***α-Diversity analysis and CANOPUS class distance computation***

01 The alpha-diversity was calculated for each species based on Shannon Entropy (Script **S29**) using
02 the scikit-bio package and sample features as OTUs. The top 252 networks as mentioned
03 previously were selected their raw peak areas summed based on propagated CANOPUS classes
04 (Script **S28**) and then converted to integers, networks without class annotations were discarded.
05 The vegan package was used to perform non-metric multidimensional scaling (NMDS) followed
06 by the calculation of intrinsic variables (CANOPUS classes) with 999 permutations (Script **S30**).
07 The resulting vectors were used to calculate the per species cosine distances (Script **S31**).
08

09 ***Code availability***

10 All scripts used in this study are available at the Github repository:
11 https://github.com/volvox292/Nicotiana_metabolomics
12

13 **Acknowledgments**

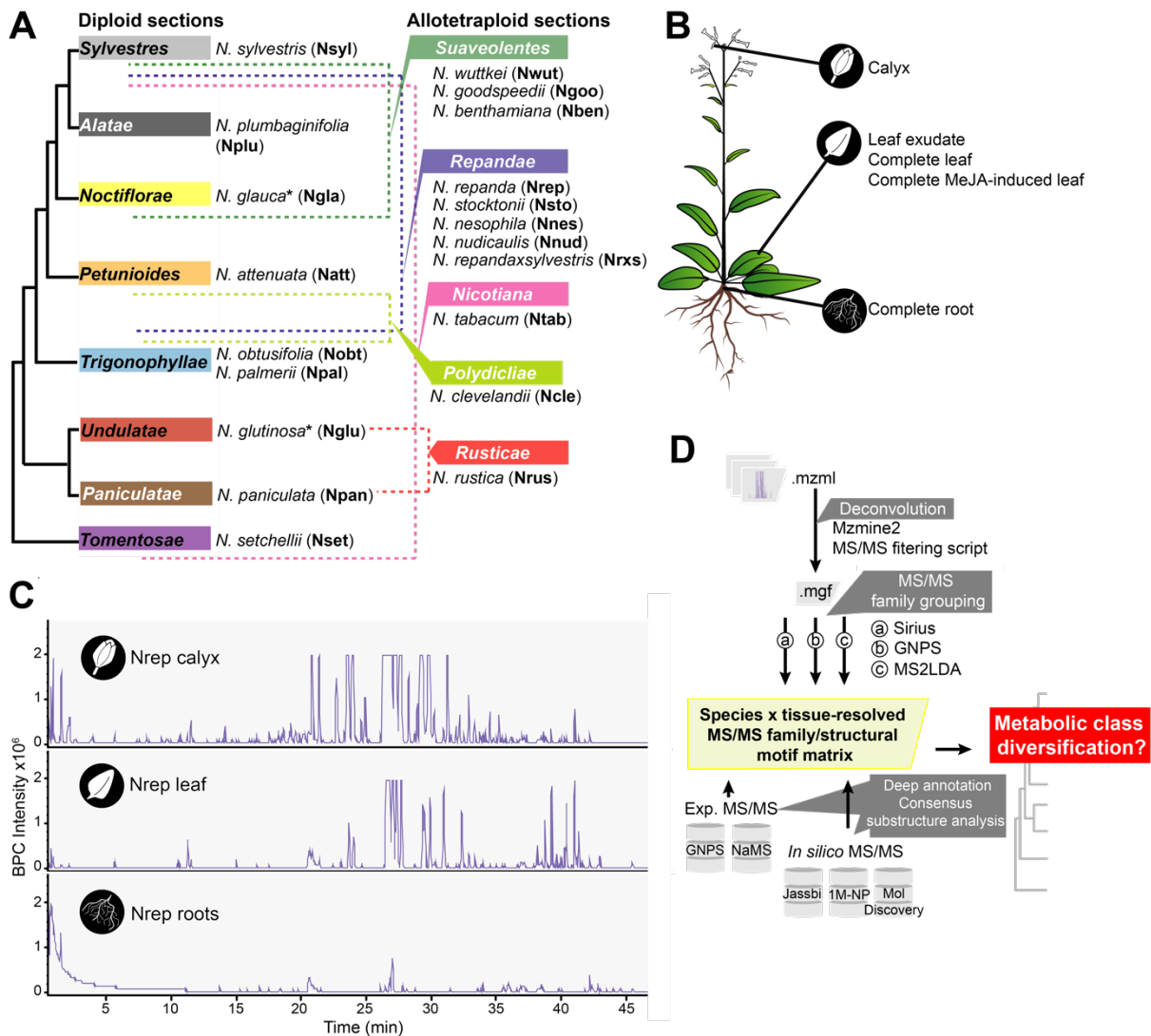
14 The authors would like to acknowledge the High Performance Computing Center of the
15 University of Strasbourg for supporting this work by providing scientific support and access to
16 computing resources. Some of these computing resources were funded by the Equipex
17 Equip@Meso project (Programme Investissements d'Avenir) and the CPER Alsacalcul/Big Data.
18 The authors thank N. Navrot and I. Grubor for comments on the manuscript, L. Malherbe for help
19 with plant sample collection, J. Zumsteg for support with preparative HPLC purifications, the
20 Plant Imaging Mass Spectrometry platform of the IBMP for instrument access, P. Dorrestein, M.
21 Wang and M. Panitchpakdi for help with the upload of the *in-silico* 1M-DB on the GNPS
22 platform. **Funding:** D.E., D.P., C.V., L. M. and E.G. were funded by the CNRS. D.E. and E.G.
23 were supported by a IdEx (Investissement d'Avenir) Grant and PhD fellowship to D.E from the
24 University of Strasbourg. Initiation of this study by E.G. was further supported within the
25 framework of the Deutsche Forschungsgemeinschaft Excellence Initiative to the University of
26 Heidelberg. **Author contributions:** D.E. and E.G. conceived the study, performed the

27 experiments, analyzed the data, and wrote the paper with inputs from the other authors. D.P.
28 contributed bioinformatics support. C.V. performed mass spectrometry measurements. B.M. and
29 L.M. performed NMR analyses. **Competing interests:** The authors declare that they have no
30 competing interests. **Data and materials availability:** Metabolomics raw data and .mzml files
31 were deposited on MassIVE <https://doi.org/doi:10.25345/C5QB9V93Q>. MSI data was deposited
32 at metaspace https://metaspace2020.eu/project/nicotiana_msi-2022. Additional data is available on
33 Zenodo <https://doi.org/10.5281/zenodo.6536010>. All scripts used in this study are available at the
34 Github repository: https://github.com/volvox292/Nicotiana_metabolomics. All data needed to
35 evaluate the conclusions in the paper are further present in the paper and/or the Supplementary
36 Materials.

37

38

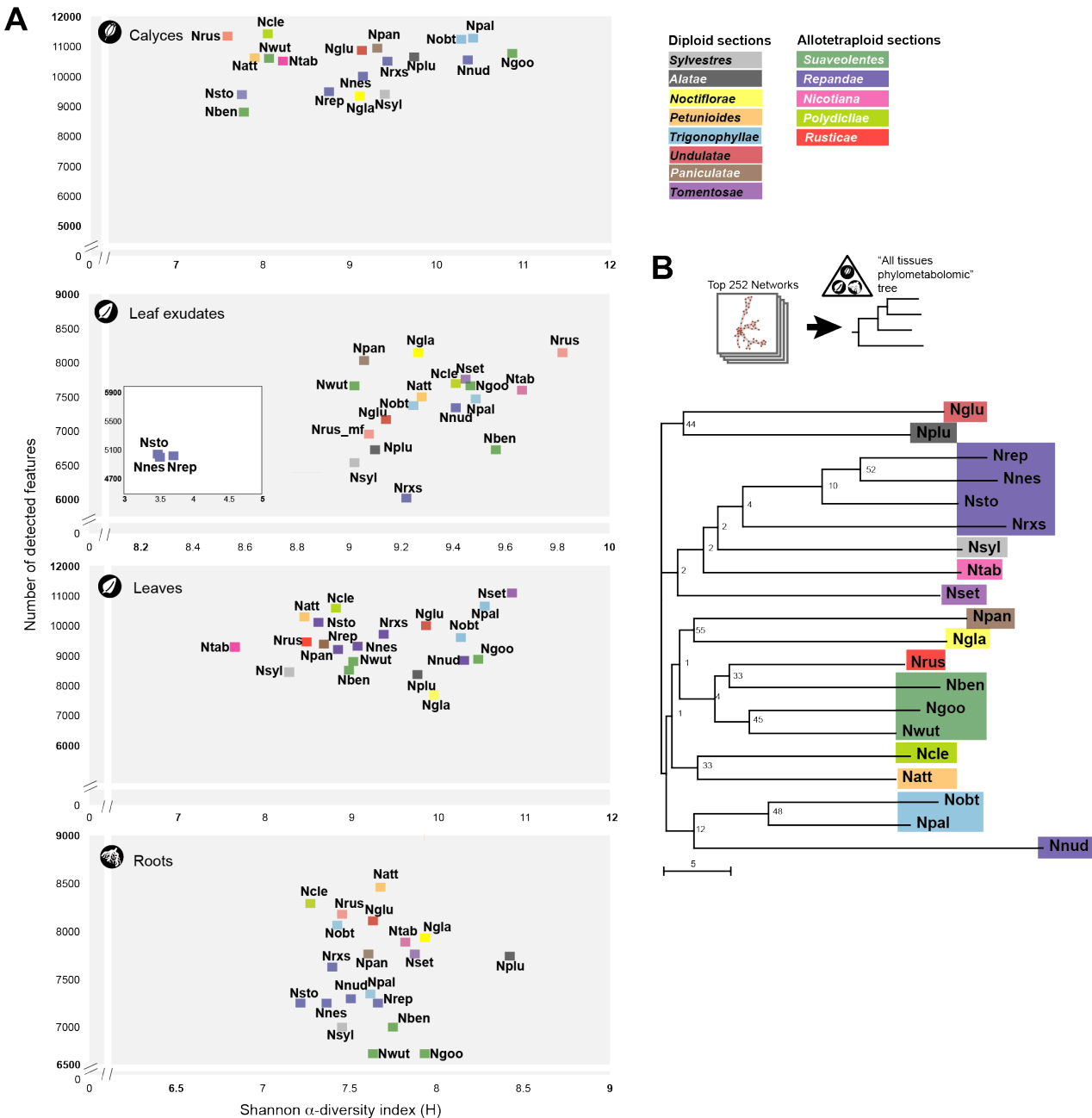
Figure 1



53

Figure 2

54

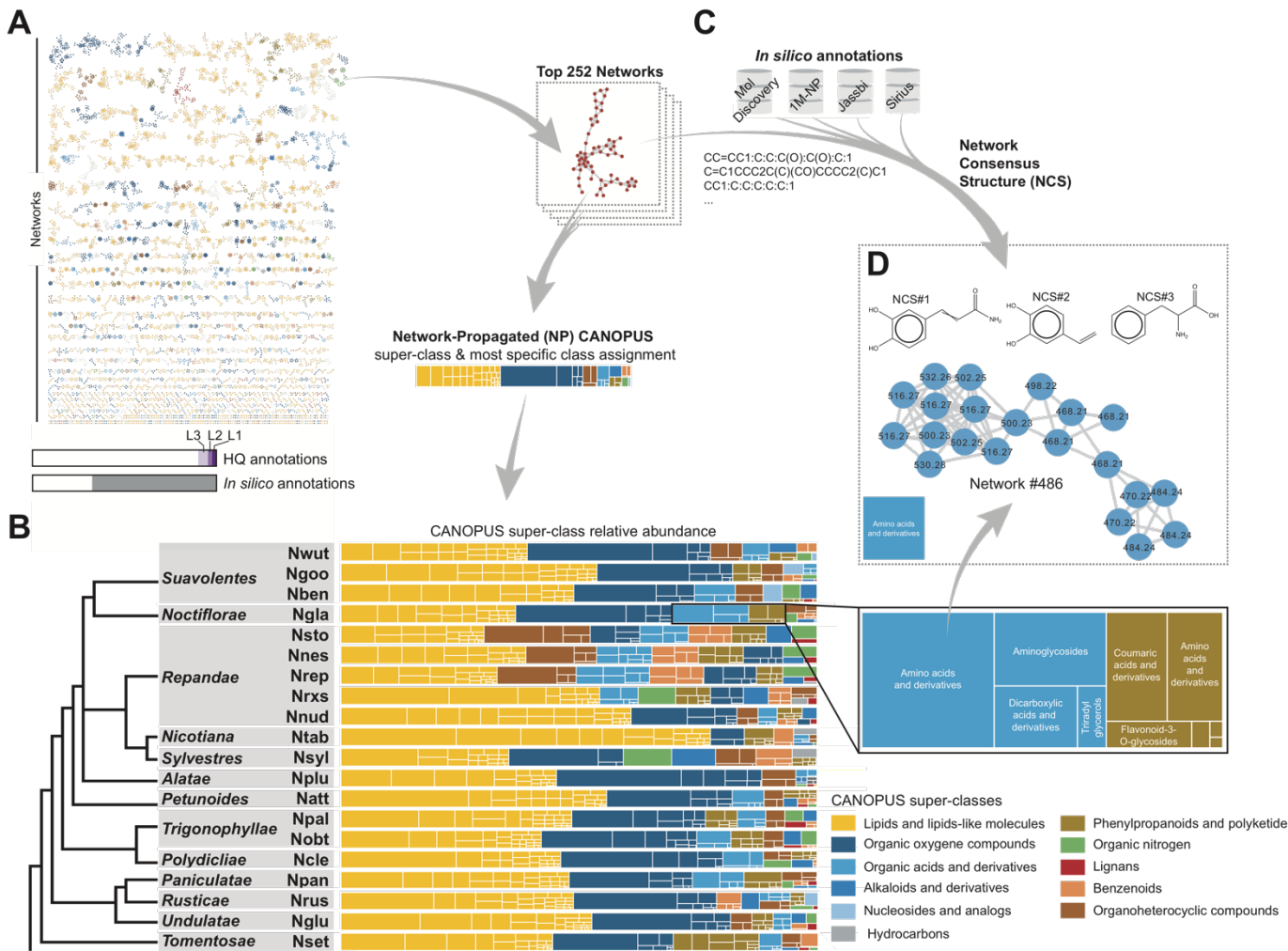


55

Figure 2. Species metabolome α -diversity and “phylogenomics” relatedness. (A) Biplots depict the number of detected features and the Information Theory Shannon α -diversity as an index of feature richness *per* tissue. *Nicotiana* phylogenetic sections are color-coded. (B) “Phylogenomics” tree computed from the molecular networking information. To analyze the relatedness of species’ metabolomes, we first computed inter-species Euclidean distances based the molecular networking information and used the resulting distance matrices for constructing a “phylogenomics” tree based on the Neighbor-Joining algorithm (bootstrap values derived from 999 iterations) (Table S2). Trees were also constructed from the tissue-level data (Fig. S4).

64
65

Figure 3

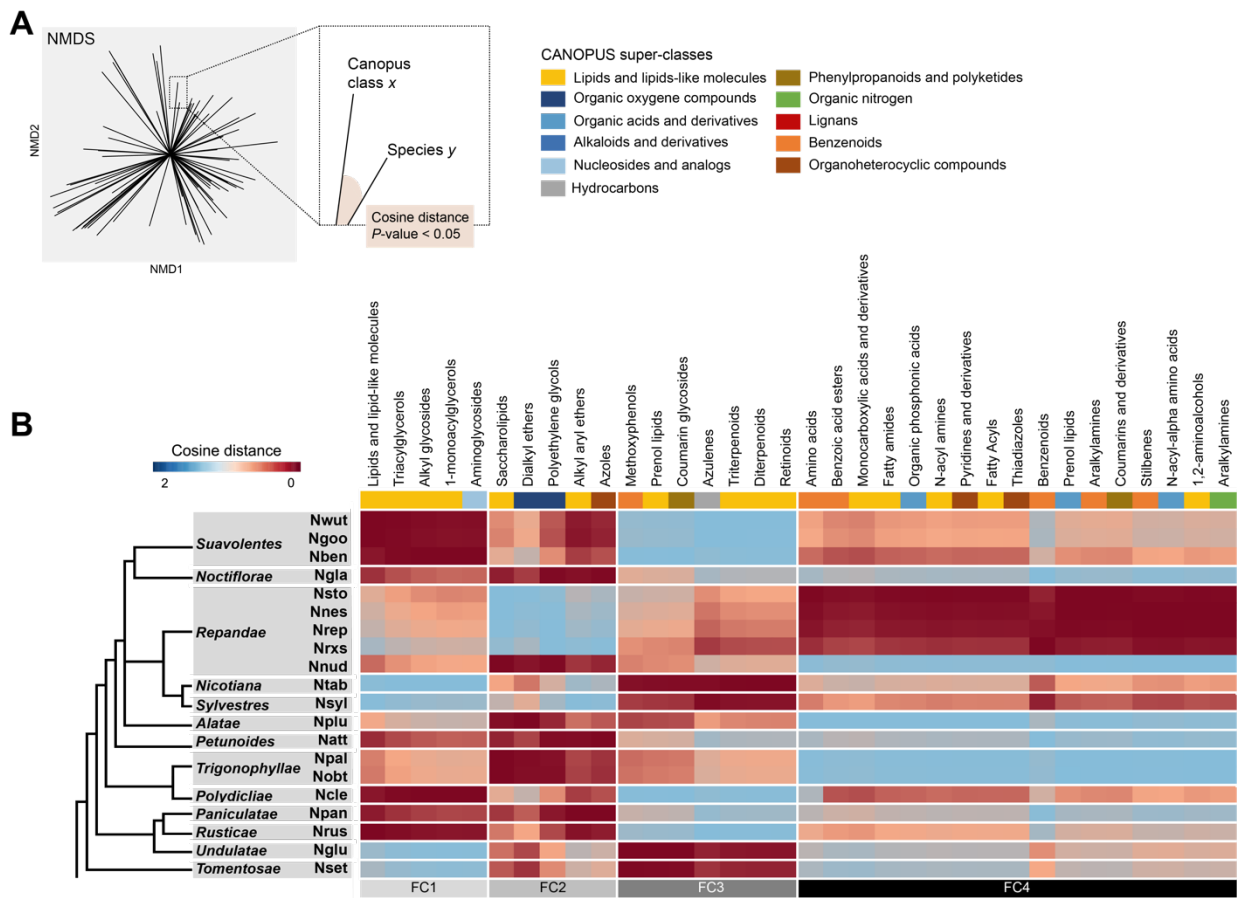


66
67
68
69
70
71
72
73
74
75
76
77
78
79
80
81
82

Figure 3. Cartography of *Nicotiana* species-level metabolic class and substructure distribution using a novel molecular network-propagated consensus substructure approach. (A) Molecular networking of species x tissue deconvoluted MS/MS features. The top252 molecular networks were retrieved for a minimum MS/MS pairwise cosine value of 0.7 and of 6 matching m/z signals. Node colors refer to network-propagated CANOPUS super-class predictions. Bars refer to the relative proportions of individual MS/MS further annotated from the three levels of annotation confidence (see **Material and Methods** section) or with databases build from *in silico* generated MS/MS spectra (see panel **C**). **(B)** Treemap visualization of species-level super-class and most specific class distribution. Colors denote for different NP-CANOPUS super-classes, with each individual uniformly colored rectangles depicting most-specific classes hierarchically classified as part of a NP-CANOPUS super-class. A close-up view on two super-classes ("Organic acids and derivatives" / "Phenylpropanoids and polyketides") detected in *N. glauca* (Ngla) is presented. **(C)** Network Consensus Structure (NCS) computations from hits obtained from the interrogation of *in silico* generated MS/MS spectra (**Fig. S10**). Hits obtained for each MS/MS feature-level database search within a network were compiled input to compute a consensus (sub)structure for each network. **(D)** NCS computed for network #486 whose MS/MS features were classified in **(A)** as those of "Amino acids and derivatives". The library of feature/network/NP-CANOPUS/NCS associations is reported in **Data S1, S3 and S4**.

83

Figure 4



84

Figure 4. Non-metric multidimensional scaling reveals main statistical trends of *Nicotiana* section and species-level metabolic specialization. (A) Non-metric multidimensional scaling (NMDS) was used to infer directionalities, followed by the calculation of intrinsic variables to test for statistical significance (P -value [999 permutations] lower or equal to 0.05), in the association between species and CANOPUS super-class and most specific class predictions (CANOPUS, Fig. 2). All P -values and cosine distances are summarized in **Data S2**. (B) Heatmap representation (based on cosine distances) of statistically significant associations between species and NP-CANOPUS predictions for “most-specific classes” (colored according to upper-level “super-classes”). A hierarchical clustering analysis was conducted to group similarly distributed CANOPUS predictions, thereby emphasizing on four highly distinctive clusters referred to as metabolic family clusters (FC).

94

95

Figure 5

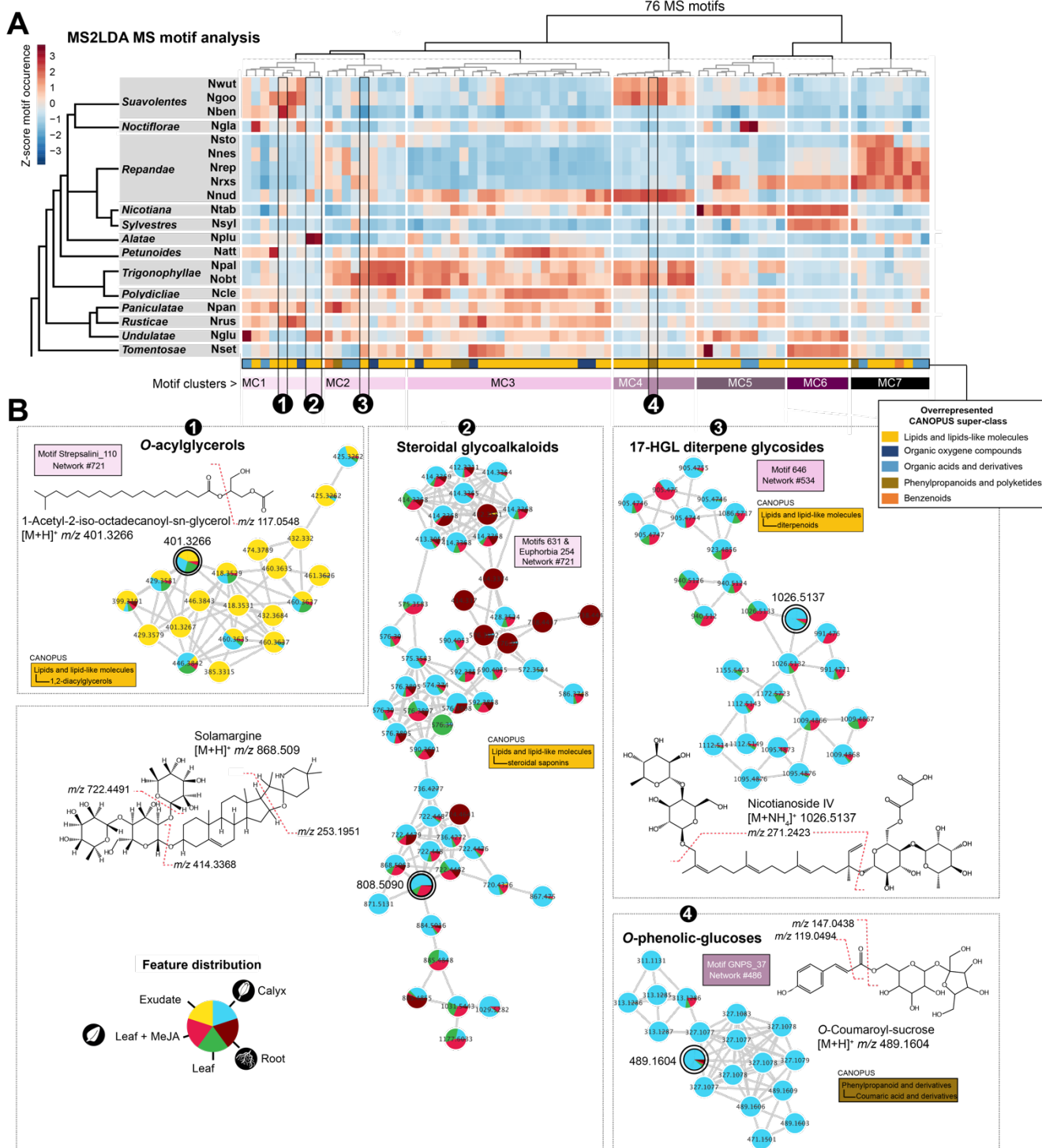
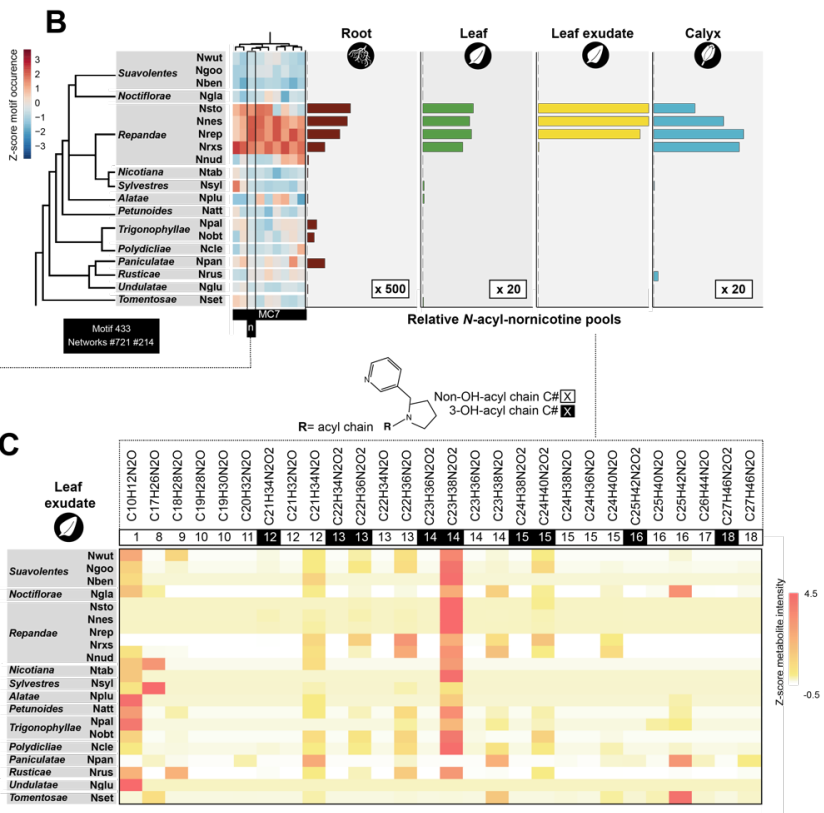
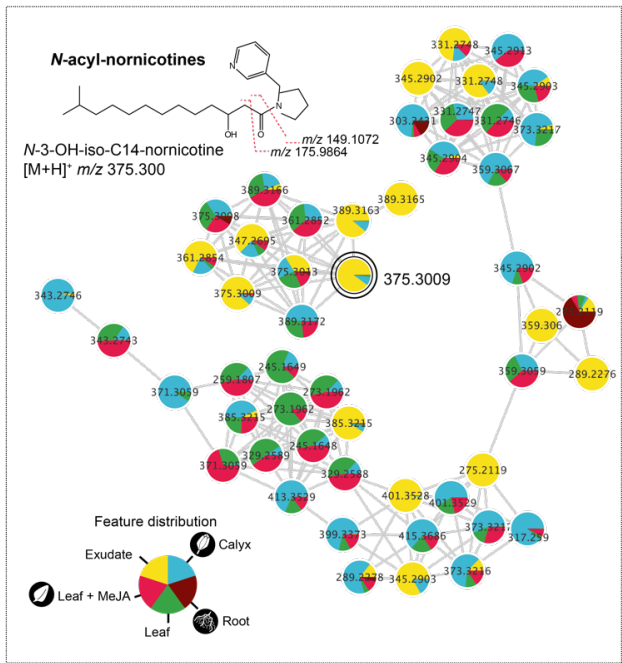


Figure 5. A minimal set of MS motifs captures substructure diversity in *Nicotiana* chemotypes. (A) Hierarchical clustering analysis (HCA) based on the species-level motif count (Z-score normalized) of top76 mass motifs inferred by unsupervised decomposition of overall MS spectra via the text-mining program MS2LDA. Species x tissue motif counts matrices can be explored within **Data S5**. Motifs clusters (MC) extracted from the HCA approach refer to clusters of tightly covarying MS motifs. A Principal Component (PC) analysis (2 first PCs) based on species-level MS motif relative intensities and loadings exerted on sample PC coordinates by each MS motifs, highlighted the strong resolving power for species grouping of these MCs (**Fig. S9**). **(B)** Strategy for MS motif-guided exploration of substructure enrichment in particular molecular networks. MS motifs are selected based on their peculiar species/section-level distribution, annotated using MS fragmentation curation and connected molecular network are

08 finally visualized. Node colors denote for the species-overall feature relative abundance in the analyzed tissues.
09 Rectangles report network and MS motif ids, their colors refer to MC. A representative high confidence predicted
10 structure per network (connected to the double circled node) is presented with annotation of the MS motif main
11 fragments. Additional examples are presented as part of **Fig. S10**. Overall MS motif data are reported in **Data S6** and
12 **S7**.

13

Figure 6

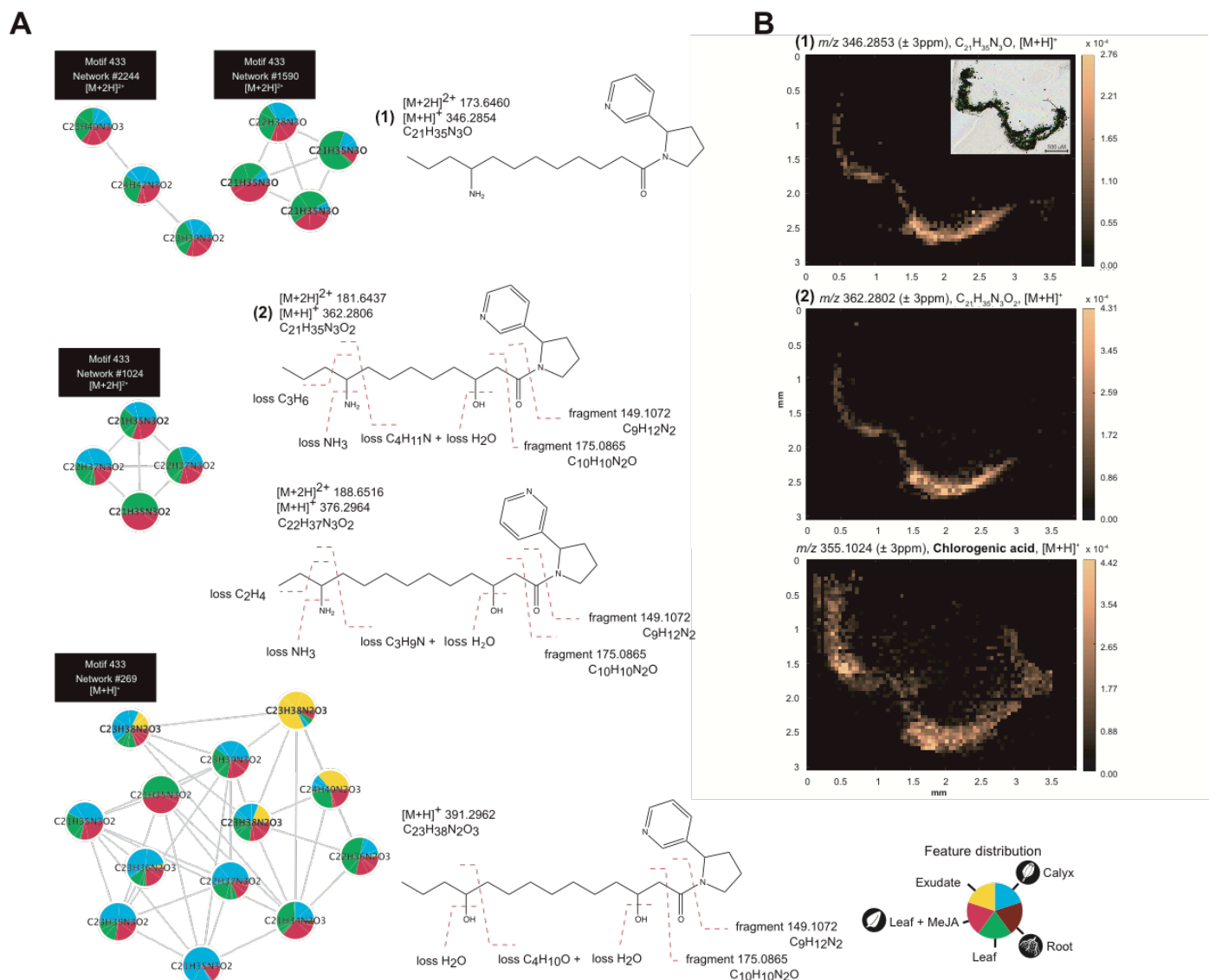


14
15
16
17
18
19
20
21
22
23
24
25

Figure 6. Navigating MS motifs pinpoints on a diversity of *N*-acylnornicotines that dominate leaf surfaces of *Nicotiana* section *Repandae* species. (A) Main molecular networks extracted connected to MS motif 433 (MC7, Fig. 5A) characterized by a strong relative abundance in *Repandae* species. NMR-elucidated *N*-acylnornicotine (NANN) structure (see further NMR-elucidated NANNs in Fig. S11), with fragment annotations captured by the NANN MS motif, for the MS/MS feature represented by the double circled node. Node colors denote for the species-overall feature relative abundance in the analyzed tissues. (B) Total NANN pools (relative to maximum in *N. nesophila* exudates) as inferred from MS/MS features of MS motif 433 (Data S8). (C) Species-level NANN elemental formula distribution (Z-score normalized) and indication of the acyl chain length and of its 3-hydroxylation.

26
27

Figure 7



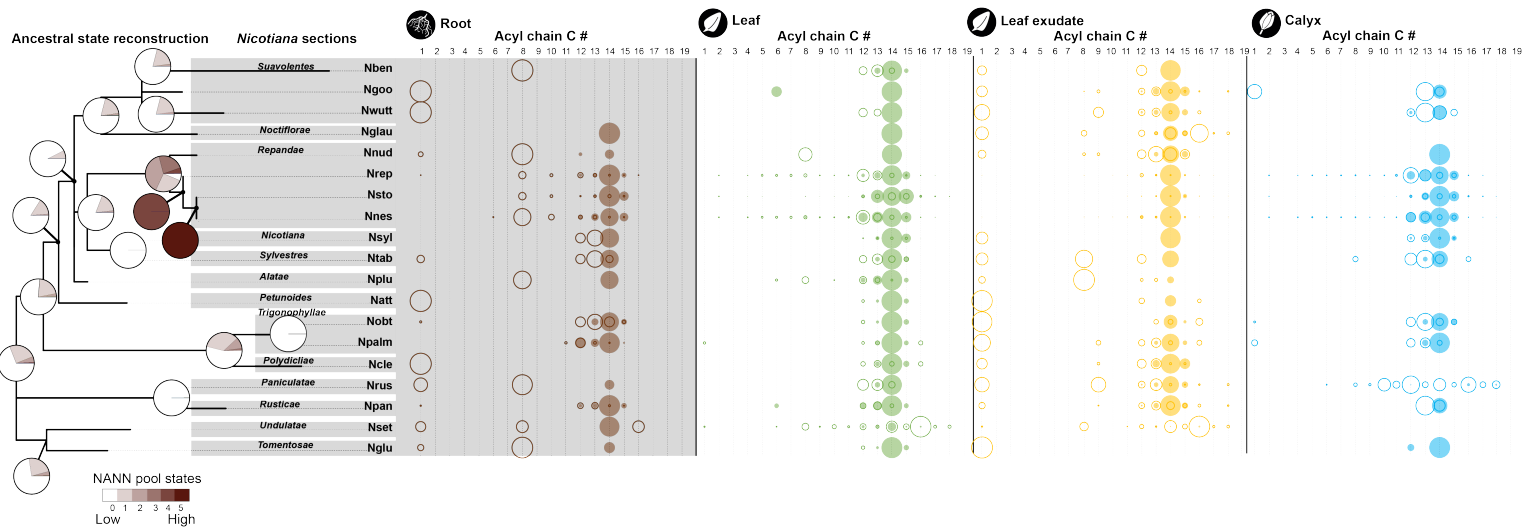
28
29
30
31
32
33
34
35
36
37
38

Figure 7. Characterization of non-canonical leaf lamina NANNs specific to the *Repandae*. (A) Molecular networks and fragmentation characterization of 3N-containing and di-hydroxylated NANN specific to the *Repandae* (Fig. S13). Node colors denote for the species-overall feature relative abundance in the analyzed tissues. (B) MALDI-MSI images depicting spatially-resolved relative abundance of selected metabolites in a leaf cross section of *N. nesophila*. Insert in the first image corresponds to the optical image of the matrix-embedded leaf cut used for MALDI-MSI. The two first images correspond to the MSI data for two 3N-containing NANNs: m/z 346.2853 (\pm 3ppm, $C_{21}H_{35}N_3O$, $[M+H]^+$) and m/z 362.2802 (\pm 3ppm, $C_{21}H_{35}N_3O_2$, $[M+H]^+$) exhibiting a quasi-uniform distribution within the complete leaf section and comparable to that of chlorogenic acid (third image, m/z 355.1026 \pm 3ppm). Selected MSI data are presented for additional *N. nesophila* metabolites in Fig. S14.

39

Figure 8

40



41

Figure 8. Ancestral state reconstruction and structural diversity analysis indicate that NANNs predate Repandae speciation and a major root-to-shoot compositional shift. Total root NANN pools of the focal species were transposed as relative scaling into an ordered trait (total states colored from white to dark brown) and used as input for ancestral state reconstruction using the MBASR software with default settings. The species tree was constructed from *matK* as described in (71). Bubble plots on the right part of the figure depicts relative NANN fatty acyl chain distribution with indication of fatty acyl chain carbon number (Fig. S12), for total NANN pools see Fig. 6B. Bubble size denote for relative acyl chain level within the NANN pool of a species and *per* tissue. Color-filled bubbles refer to hydroxylated NANNs.

50

51

52

53 **References**

- 54 1. H. A. Maeda, A. R. Fernie, Evolutionary History of Plant Metabolism. *Annu. Rev. Plant*
55 *Biol.* **72**, 185–216 (2021).
- 56 2. M. Pigliucci, Phenotypic integration: studying the ecology and evolution of complex
57 phenotypes. *Ecology Letters*. **6**, 265–272 (2003).
- 58 3. S. R. Whitehead, E. Bass, A. Corrigan, A. Kessler, K. Poveda, Interaction diversity explains
59 the maintenance of phytochemical diversity. *Ecology Letters*. **24**, 1205–1214 (2021).
- 60 4. D. Li, E. Gaquerel, Next-Generation Mass Spectrometry Metabolomics Revives the
61 Functional Analysis of Plant Metabolic Diversity. *Annual Review of Plant Biology*. **72**, 867–
62 891 (2021).
- 63 5. K. B. Kang, M. Ernst, J. J. J. van der Hooft, R. R. da Silva, J. Park, M. H. Medema, S. H.
64 Sung, P. C. Dorrestein, Comprehensive mass spectrometry-guided phenotyping of plant
65 specialized metabolites reveals metabolic diversity in the cosmopolitan plant family
66 Rhamnaceae. *The Plant Journal*. **98**, 1134–1144 (2019).
- 67 6. S. Heiling, S. Khanal, A. Barsch, G. Zurek, I. T. Baldwin, E. Gaquerel, Using the knowns to
68 discover the unknowns: MS-based dereplication uncovers structural diversity in 17-
69 hydroxygeranylinalool diterpene glycoside production in the Solanaceae. *The Plant*
70 *Journal*. **85**, 561–577 (2016).
- 71 7. M. Itkin, U. Heinig, O. Tzfadia, A. J. Bhide, B. Shinde, P. D. Cardenas, S. E. Bocobza, T.
72 Unger, S. Malitsky, R. Finkers, Y. Tikunov, A. Bovy, Y. Chikate, P. Singh, I. Rogachev, J.
73 Beekwilder, A. P. Giri, A. Aharoni, Biosynthesis of Antinutritional Alkaloids in
74 Solanaceous Crops Is Mediated by Clustered Genes. *Science*. **341**, 175–179 (2013).
- 75 8. D. Li, S. Heiling, I. T. Baldwin, E. Gaquerel, Illuminating a plant's tissue-specific metabolic
76 diversity using computational metabolomics and information theory. *Proceedings of the*
77 *National Academy of Sciences*. **113**, E7610–E7618 (2016).
- 78 9. S. Meldau, M. Erb, I. T. Baldwin, Defence on demand: mechanisms behind optimal defence
79 patterns. *Annals of Botany*. **110**, 1503–1514 (2012).
- 80 10. R. Schuurink, A. Tissier, Glandular trichomes: micro-organs with model status? *New*
81 *Phytologist*. **225**, 2251–2266 (2020).
- 82 11. G. D. Moghe, B. J. Leong, S. M. Hurney, A. Daniel Jones, R. L. Last, Evolutionary routes to
83 biochemical innovation revealed by integrative analysis of a plant-defense related
84 specialized metabolic pathway. *eLife*. **6**, e28468 (2017).
- 85 12. O. Servettaz, A. Pinetti, F. Bellesia, L. B. Maleci, Micromorphological and Phytochemical
86 Research on *Teucrium scorodonia* and *Teucrium siculum* from the Italian Flora. *Botanica*
87 *Acta*. **107**, 416–421 (1994).
- 88 13. Y. Sun, T. Guo, F. Zhang, Y. Wang, Z. Liu, S. Guo, L. Li, Isolation and characterization of
89 cytotoxic withanolides from the calyx of *Physalis alkekengi* L. var *franchetii*. *Bioorganic*
90 *Chemistry*. **96**, 103614 (2020).

91 14. S. J. Livingston, T. D. Quilichini, J. K. Booth, D. C. J. Wong, K. H. Rensing, J. Laflamme-
92 Yonkman, S. D. Castellarin, J. Bohlmann, J. E. Page, A. L. Samuels, *Cannabis* glandular
93 trichomes alter morphology and metabolite content during flower maturation. *The Plant*
94 *Journal*. **101**, 37–56 (2020).

95 15. E. Korenblum, Y. Dong, J. Szymanski, S. Panda, A. Jozwiak, H. Massalha, S. Meir, I.
96 Rogachev, A. Aharoni, Rhizosphere microbiome mediates systemic root metabolite
97 exudation by root-to-root signaling. *Proceedings of the National Academy of Sciences*. **117**,
98 3874–3883 (2020).

99 16. A. C. Huang, T. Jiang, Y.-X. Liu, Y.-C. Bai, J. Reed, B. Qu, A. Goossens, H.-W. Nützmann,
00 Y. Bai, A. Osbourn, A specialized metabolic network selectively modulates *Arabidopsis* root
01 microbiota. *Science*. **364**, eaau6389 (2019).

02 17. A. A. Aksенов, R. da Silva, R. Knight, N. P. Lopes, P. C. Dorrestein, Global chemical
03 analysis of biology by mass spectrometry. *Nat Rev Chem*. **1**, 0054 (2017).

04 18. L.-F. Nothias, D. Petras, R. Schmid, K. Dührkop, J. Rainer, A. Sarvepalli, I. Protsyuk, M.
05 Ernst, H. Tsugawa, M. Fleischauer, F. Aicheler, A. A. Aksenov, O. Alka, P.-M. Allard, A.
06 Barsch, X. Cachet, A. M. Caraballo-Rodriguez, R. R. Da Silva, T. Dang, N. Garg, J. M.
07 Gauglitz, A. Gurevich, G. Isaac, A. K. Jarmusch, Z. Kameník, K. B. Kang, N. Kessler, I.
08 Koester, A. Korf, A. Le Gouellec, M. Ludwig, C. Martin H., L.-I. McCall, J. McSayles, S.
09 W. Meyer, H. Mohimani, M. Morsy, O. Moyne, S. Neumann, H. Neuweiger, N. H. Nguyen,
10 M. Nothias-Esposito, J. Paolini, V. V. Phelan, T. Pluskal, R. A. Quinn, S. Rogers, B.
11 Shrestha, A. Tripathi, J. J. J. van der Hooft, F. Vargas, K. C. Weldon, M. Witting, H. Yang,
12 Z. Zhang, F. Zubeil, O. Kohlbacher, S. Böcker, T. Alexandrov, N. Bandeira, M. Wang, P. C.
13 Dorrestein, Feature-based molecular networking in the GNPS analysis environment. *Nat*
14 *Methods*. **17**, 905–908 (2020).

15 19. M. Wang, J. J. Carver, V. V. Phelan, L. M. Sanchez, N. Garg, Y. Peng, D. D. Nguyen, J.
16 Watrous, C. A. Kapono, T. Luzzatto-Knaan, C. Porto, A. Bouslimani, A. V. Melnik, M. J.
17 Meehan, W.-T. Liu, M. Crüsemann, P. D. Boudreau, E. Esquenazi, M. Sandoval-Calderón,
18 R. D. Kersten, L. A. Pace, R. A. Quinn, K. R. Duncan, C.-C. Hsu, D. J. Floros, R. G.
19 Gavilan, K. Kleigrewe, T. Northen, R. J. Dutton, D. Parrot, E. E. Carlson, B. Aigle, C. F.
20 Michelsen, L. Jelsbak, C. Sohlenkamp, P. Pevzner, A. Edlund, J. McLean, J. Piel, B. T.
21 Murphy, L. Gerwick, C.-C. Liaw, Y.-L. Yang, H.-U. Humpf, M. Maansson, R. A. Keyzers,
22 A. C. Sims, A. R. Johnson, A. M. Sidebottom, B. E. Sedio, A. Klitgaard, C. B. Larson, C. A.
23 Boya P, D. Torres-Mendoza, D. J. Gonzalez, D. B. Silva, L. M. Marques, D. P. Demarque,
24 E. Pociute, E. C. O'Neill, E. Briand, E. J. N. Helfrich, E. A. Granatosky, E. Glukhov, F.
25 Ryffel, H. Houson, H. Mohimani, J. J. Kharbush, Y. Zeng, J. A. Vorholt, K. L. Kurita, P.
26 Charusanti, K. L. McPhail, K. F. Nielsen, L. Vuong, M. Elfeki, M. F. Traxler, N. Engene, N.
27 Koyama, O. B. Vining, R. Baric, R. R. Silva, S. J. Mascuch, S. Tomasi, S. Jenkins, V.
28 Macherla, T. Hoffman, V. Agarwal, P. G. Williams, J. Dai, R. Neupane, J. Gurr, A. M. C.
29 Rodríguez, A. Lamsa, C. Zhang, K. Dorrestein, B. M. Duggan, J. Almaliti, P.-M. Allard, P.
30 Phapale, L.-F. Nothias, T. Alexandrov, M. Litaudon, J.-L. Wolfender, J. E. Kyle, T. O.
31 Metz, T. Peryea, D.-T. Nguyen, D. VanLeer, P. Shinn, A. Jadhav, R. Müller, K. M. Waters,
32 W. Shi, X. Liu, L. Zhang, R. Knight, P. R. Jensen, B. Ø. Palsson, K. Pogliano, R. G.
33 Linington, M. Gutiérrez, N. P. Lopes, W. H. Gerwick, B. S. Moore, P. C. Dorrestein, N.
34 Bandeira, Sharing and community curation of mass spectrometry data with Global Natural
35 Products Social Molecular Networking. *Nature Biotechnology*. **34**, 828–837 (2016).

36 20. K. Dührkop, L.-F. Nothias, M. Fleischauer, R. Reher, M. Ludwig, M. A. Hoffmann, D.
37 Petras, W. H. Gerwick, J. Rousu, P. C. Dorrestein, S. Böcker, Systematic classification of
38 unknown metabolites using high-resolution fragmentation mass spectra. *Nat Biotechnol.* **39**,
39 462–471 (2021).

40 21. K. Dührkop, M. Fleischauer, M. Ludwig, A. A. Aksенов, A. V. Melnik, M. Meusel, P. C.
41 Dorrestein, J. Rousu, S. Böcker, SIRIUS 4: a rapid tool for turning tandem mass spectra into
42 metabolite structure information. *Nature Methods.* **16**, 299–302 (2019).

43 22. J. Wandy, Y. Zhu, J. J. J. van der Hooft, R. Daly, M. P. Barrett, S. Rogers, Ms2lda.org: web-
44 based topic modelling for substructure discovery in mass spectrometry. *Bioinformatics.* **34**,
45 317–318 (2018).

46 23. F. Wang, J. Liigand, S. Tian, D. Arndt, R. Greiner, D. S. Wishart, CFM-ID 4.0: More
47 Accurate ESI-MS/MS Spectral Prediction and Compound Identification. *Anal. Chem.* **93**,
48 11692–11700 (2021).

49 24. L. Cao, M. Guler, A. Tagirdzhanov, Y.-Y. Lee, A. Gurevich, H. Mohimani, MolDiscovery:
50 learning mass spectrometry fragmentation of small molecules. *Nat Commun.* **12**, 3718
51 (2021).

52 25. C. Ruttkies, E. L. Schymanski, S. Wolf, J. Hollender, S. Neumann, MetFrag relaunched:
53 incorporating strategies beyond in silico fragmentation. *Journal of Cheminformatics.* **8**, 3
54 (2016).

55 26. J. Koopman, S. Grimme, From QCEIMS to QCxMS: A Tool to Routinely Calculate CID
56 Mass Spectra Using Molecular Dynamics. *J. Am. Soc. Mass Spectrom.* **32**, 1735–1751
57 (2021).

58 27. S. Knapp, M. W. Chase, J. J. Clarkson, Nomenclatural changes and a new sectional
59 classification in *Nicotiana* (Solanaceae). *Taxon.* **53**, 73–82 (2004).

60 28. POWO, Plants of the World Online. Facilitated by the Royal Botanic Gardens, Kew.
61 Published on the Internet. *Plants of the World Online* (2022), (available at
62 <http://www.plantsoftheworldonline.org/>).

63 29. B. Usade, T. Tohge, F. Scossa, N. Sierro, M. Schmidt, A. Vogel, A. Bolger, A. Kozlo, E. M.
64 Enfissi, K. Morrel, M. Regenauer, A. Hallab, C. Ruprecht, H. Gundlach, M. Spannagl, Y.
65 Koram, K. F. Mayer, W. Boerjan, P. D. Fraser, S. Persson, N. V. Ivanov, A. R. Fernie, The
66 genome and metabolome of the tobacco tree, *Nicotiana glauca*: a potential renewable
67 feedstock for the bioeconomy (2018), p. 351429.

68 30. M. A. Pombo, H. G. Rosli, N. Fernandez-Pozo, A. Bombara, "Nicotiana benthamiana, A
69 Popular Model for Genome Evolution and Plant–Pathogen Interactions" in *The Tobacco*
70 *Plant Genome*, N. V. Ivanov, N. Sierro, M. C. Peitsch, Eds. (Springer International
71 Publishing, Cham, 2020; https://doi.org/10.1007/978-3-030-29493-9_14), *Compendium of*
72 *Plant Genomes*, pp. 231–247.

73 31. H. Foerster, L. A. Mueller, "Tobacco Resources in the Sol Genomics Network and Nicotiana
74 Metabolic Databases" in *The Tobacco Plant Genome*, N. V. Ivanov, N. Sierro, M. C.
75 Peitsch, Eds. (Springer International Publishing, Cham, 2020; https://doi.org/10.1007/978-3-030-29493-9_5), *Compendium of Plant Genomes*, pp. 59–71.

77 32. A. R. Jassbi, S. Zare, M. Asadollahi, M. C. Schuman, Ecological Roles and Biological
78 Activities of Specialized Metabolites from the Genus *Nicotiana*. *Chem. Rev.* **117**, 12227–
79 12280 (2017).

80 33. A. Navarro-Quezada, K. Gase, R. K. Singh, S. P. Pandey, I. T. Baldwin, "Nicotiana
81 attenuata Genome Reveals Genes in the Molecular Machinery Behind Remarkable Adaptive
82 Phenotypic Plasticity" in *The Tobacco Plant Genome*, N. V. Ivanov, N. Sierro, M. C.
83 Peitsch, Eds. (Springer International Publishing, Cham, 2020; https://doi.org/10.1007/978-3-030-29493-9_13), *Compendium of Plant Genomes*, pp. 211–229.

85 34. E. W. McCarthy, M. W. Chase, S. Knapp, A. Litt, A. R. Leitch, S. C. Le Comber,
86 Transgressive phenotypes and generalist pollination in the floral evolution of *Nicotiana*
87 polyploids. *Nature Plants*. **2**, 1–9 (2016).

88 35. R. F. Severson, J. E. Huesing, D. Jones, R. F. Arrendale, V. A. Sisson, Identification of
89 tobacco hornworm antibiosis factor from cuticulae of *Repandae* section of *Nicotiana*
90 species. *J Chem Ecol.* **14**, 1485–1494 (1988).

91 36. G. Laue, C. A. Preston, I. T. Baldwin, Fast track to the trichome: induction of N-acyl
92 nornicotines precedes nicotine induction in *Nicotiana repanda*. *Planta*. **210**, 510–514
93 (2000).

94 37. R. F. Severson, R. F. Arrendale, H. G. Cutler, D. Jones, V. A. Sisson, M. G. Stephenson,
95 "Chemistry and Biological Activity of Acylnornicotines from *Nicotiana repanda*" in
96 *Biologically Active Natural Products* (American Chemical Society, 1988;
97 <https://doi.org/10.1021/bk-1988-0380.ch022>), vol. 380 of *ACS Symposium Series*, pp. 335–
98 362.

99 38. J. E. Huesing, D. Jones, A new form of antibiosis in *Nicotiana*. *Phytochemistry*. **26**, 1381–
00 1384 (1987).

01 39. N. Onkokesung, E. Gaquerel, H. Kotkar, H. Kaur, I. T. Baldwin, I. Galis, MYB8 Controls
02 Inducible Phenolamide Levels by Activating Three Novel Hydroxycinnamoyl-Coenzyme
03 A:Polyamine Transferases in *Nicotiana attenuata*. *Plant Physiology*. **158**, 389–407 (2012).

04 40. M. A. Beniddir, K. Bin Kang, G. Genta-Jouve, F. Huber, S. Rogers, J. J. J. van der Hooft,
05 Advances in decomposing complex metabolite mixtures using substructure- and network-
06 based computational metabolomics approaches. *Natural Product Reports*. **38**, 1967–1993
07 (2021).

08 41. L. W. Sumner, A. Amberg, D. Barrett, M. H. Beale, R. Beger, C. A. Daykin, T. W.-M. Fan,
09 O. Fiehn, R. Goodacre, J. L. Griffin, T. Hankemeier, N. Hardy, J. Harnly, R. Higashi, J.
10 Kopka, A. N. Lane, J. C. Lindon, P. Marriott, A. W. Nicholls, M. D. Reily, J. J. Thaden, M.
11 R. Viant, Proposed minimum reporting standards for chemical analysis. *Metabolomics*. **3**,
12 211–221 (2007).

13 42. P.-M. Allard, T. Péresse, J. Bisson, K. Gindro, L. Marcourt, V. C. Pham, F. Roussi, M.
14 Litaudon, J.-L. Wolfender, Integration of Molecular Networking and *In-Silico* MS/MS
15 Fragmentation for Natural Products Dereplication. *Anal. Chem.* **88**, 3317–3323 (2016).

16 43. H. W. Kim, M. Wang, C. A. Leber, L.-F. Nothias, R. Reher, K. B. Kang, J. J. J. van der
17 Hooft, P. C. Dorrestein, W. H. Gerwick, G. W. Cottrell, NPClassifier: A Deep Neural

18 Network-Based Structural Classification Tool for Natural Products. *J Nat Prod.* **84**, 2795–
19 2807 (2021).

20 44. P. L. Buttigieg, A. Ramette, A guide to statistical analysis in microbial ecology: a
21 community-focused, living review of multivariate data analyses. *FEMS Microbiology
22 Ecology*. **90**, 543–550 (2014).

23 45. M. Ernst, K. B. Kang, A. M. Caraballo-Rodríguez, L.-F. Nothias, J. Wandy, C. Chen, M.
24 Wang, S. Rogers, M. H. Medema, P. C. Dorrestein, J. J. J. van der Hooft, MolNetEnhancer:
25 Enhanced Molecular Networks by Integrating Metabolome Mining and Annotation Tools.
26 *Metabolites*. **9**, 144 (2019).

27 46. E. Gaquerel, C. Kuhl, S. Neumann, Computational annotation of plant metabolomics
28 profiles via a novel network-assisted approach. *Metabolomics*. **9**, 904–918 (2013).

29 47. S. Li, Y. Park, S. Duraisingham, F. H. Strobel, N. Khan, Q. A. Soltow, D. P. Jones, B.
30 Pulendran, Predicting Network Activity from High Throughput Metabolomics. *PLOS
31 Computational Biology*. **9**, e1003123 (2013).

32 48. N. F. de Jonge, J. R. Louwen, E. Chekmeneva, S. Camuzeaux, F. J. Vermeir, R. S. Jansen, F.
33 Huber, J. J. J. van der Hooft, MS2Query: Reliable and Scalable MS2 Mass Spectral-based
34 Analogue Search (2022), p. 2022.07.22.501125, , doi:10.1101/2022.07.22.501125.

35 49. A. Young, B. Wang, H. Röst, MassFormer: Tandem Mass Spectrum Prediction with Graph
36 Transformers (2021), (available at <http://arxiv.org/abs/2111.04824>).

37 50. M. A. Hoffmann, L.-F. Nothias, M. Ludwig, M. Fleischauer, E. C. Gentry, M. Witting, P. C.
38 Dorrestein, K. Dührkop, S. Böcker, High-confidence structural annotation of metabolites
39 absent from spectral libraries. *Nat Biotechnol.* **40**, 411–421 (2022).

40 51. M. Drapal, E. M. A. Enfissi, P. D. Fraser, The chemotype core collection of genus
41 Nicotiana. *The Plant Journal*. **n/a** (2022), doi:10.1111/tpj.15745.

42 52. H. Mannochio-Russo, R. F. de Almeida, W. D. G. Nunes, P. C. P. Bueno, A. M. Caraballo-
43 Rodríguez, A. Bauermeister, P. C. Dorrestein, V. S. Bolzani, Untargeted Metabolomics
44 Sheds Light on the Diversity of Major Classes of Secondary Metabolites in the
45 Malpighiaceae Botanical Family. *Front Plant Sci.* **13**, 854842 (2022).

46 53. D. Li, R. Halitschke, I. T. Baldwin, E. Gaquerel, Information theory tests critical predictions
47 of plant defense theory for specialized metabolism. *Science Advances*. **6**, eaaz0381 (2020).

48 54. W. Zhou, T. Brockmöller, Z. Ling, A. Omdahl, I. T. Baldwin, S. Xu, Evolution of herbivore-
49 induced early defense signaling was shaped by genome-wide duplications in *Nicotiana*.
50 *eLife*. **5**, e19531.

51 55. N. Murata, Y. Tasaka, Glycerol-3-phosphate acyltransferase in plants. *Biochimica et
52 Biophysica Acta (BBA) - Lipids and Lipid Metabolism*. **1348**, 10–16 (1997).

53 56. T. Asai, N. Hara, S. Kobayashi, S. Kohshima, Y. Fujimoto, Acylglycerols (=Glycerides)
54 from the Glandular Trichome Exudate on the Leaves of *Paulownia tomentosa*. *Helvetica
55 Chimica Acta*. **92**, 1473–1494 (2009).

56 57. T. Matsuzaki, Y. Shinozaki, M. Hagimori, T. Tobita, H. Shigematsu, A. Koiwai, Novel
57 Glycerolipids and Glycolipids from the Surface Lipids of *Nicotiana benthamiana*.
58 *Bioscience, Biotechnology, and Biochemistry*. **56**, 1565–1569 (1992).

59 58. H. Feng, L. Acosta-Gamboa, L. H. Kruse, J. D. Tracy, S. H. Chung, A. R. Nava Fereira, S.
60 Shakir, H. Xu, G. Sunter, M. A. Gore, C. L. Casteel, G. D. Moghe, G. Jander, Acylsugars
61 protect *Nicotiana benthamiana* against insect herbivory and desiccation. *Plant Mol Biol.*
62 **109**, 505–522 (2022).

63 59. H. Ennajdaoui, G. Vachon, C. Giacalone, I. Besse, C. Sallaud, M. Herzog, A. Tissier,
64 Trichome specific expression of the tobacco (*Nicotiana sylvestris*) cembratrien-ol synthase
65 genes is controlled by both activating and repressing cis-regions. *Plant Mol Biol.* **73**, 673–
66 685 (2010).

67 60. S. Singh, N. M. Khanna, M. M. Dhar, Solaplumbin, a new anticancer glycoside from
68 *Nicotiana plumbaginifolia*. *Phytochemistry*. **13**, 2020–2022 (1974).

69 61. V. Sisson, R. Severson, Alkaloid Composition of the *Nicotiana* Species. *Beiträge zur
70 Tabakforschung International/Contributions to Tobacco Research*. **14**, 327–339 (1990).

71 62. M. V. Djordjevic, L. P. Bush, S. L. Gay, H. R. Burton, Accumulation and distribution of
72 acylated nornicotine derivatives in flue-cured tobacco alkaloid isolines. *J. Agric. Food
73 Chem.* **38**, 347–350 (1990).

74 63. N. S. Outchkourov, C. A. Carollo, V. Gomez-Roldan, R. C. H. de Vos, D. Bosch, R. D. Hall,
75 J. Beekwilder, Control of anthocyanin and non-flavonoid compounds by anthocyanin-
76 regulating MYB and bHLH transcription factors in *Nicotiana benthamiana* leaves. *Front.
77 Plant Sci.* **5** (2014), doi:10.3389/fpls.2014.00519.

78 64. K. P. Kaminski, L. Bovet, H. Laparra, G. Lang, D. De Palo, N. Sierro, S. Goepfert, N. V.
79 Ivanov, Alkaloid chemophenetics and transcriptomics of the *Nicotiana* genus.
80 *Phytochemistry*. **177**, 112424 (2020).

81 65. E. Zador, D. Jones, The Biosynthesis of a Novel Nicotine Alkaloid in the Trichomes of
82 *Nicotiana stocktonii*. *Plant Physiology*. **82**, 479–484 (1986).

83 66. M. T. Bokhart, M. Nazari, K. P. Garrard, D. C. Muddiman, MSiReader v1.0: Evolving
84 Open-Source Mass Spectrometry Imaging Software for Targeted and Untargeted Analyses.
85 *J. Am. Soc. Mass Spectrom.* **29**, 8–16 (2018).

86 67. M. C. Chambers, B. Maclean, R. Burke, D. Amodei, D. L. Ruderman, S. Neumann, L.
87 Gatto, B. Fischer, B. Pratt, J. Egertson, K. Hoff, D. Kessner, N. Tasman, N. Shulman, B.
88 Frewen, T. A. Baker, M.-Y. Brusniak, C. Paulse, D. Creasy, L. Flashner, K. Kani, C.
89 Moulding, S. L. Seymour, L. M. Nuwaysir, B. Lefebvre, F. Kuhlmann, J. Roark, P. Rainer,
90 S. Detlev, T. Hemenway, A. Huhmer, J. Langridge, B. Connolly, T. Chadick, K. Holly, J.
91 Eckels, E. W. Deutsch, R. L. Moritz, J. E. Katz, D. B. Agus, M. MacCoss, D. L. Tabb, P.
92 Mallick, A cross-platform toolkit for mass spectrometry and proteomics. *Nature
93 Biotechnology*. **30**, 918–920 (2012).

94 68. T. Pluskal, S. Castillo, A. Villar-Briones, M. Oresic, MZmine 2: modular framework for
95 processing, visualizing, and analyzing mass spectrometry-based molecular profile data.
96 *BMC Bioinformatics*. **11**, 395 (2010).

97 69. J. Chong, D. S. Wishart, J. Xia, Using MetaboAnalyst 4.0 for Comprehensive and
98 Integrative Metabolomics Data Analysis. *Current Protocols in Bioinformatics*. **68**, e86
99 (2019).

00 70. F. Huber, S. Verhoeven, C. Meijer, H. Spreeuw, E. M. V. Castilla, C. Geng, J. J. J. van der
01 Hooft, S. Rogers, A. Belloum, F. Diblen, J. H. Spaaks, matchms - processing and similarity
02 evaluation of mass spectrometry data. *Journal of Open Source Software*. **5**, 2411 (2020).

03 71. J. J. Clarkson, S. Knapp, V. F. Garcia, R. G. Olmstead, A. R. Leitch, M. W. Chase,
04 Phylogenetic relationships in *Nicotiana* (Solanaceae) inferred from multiple plastid DNA
05 regions. *Molecular Phylogenetics and Evolution*, **16** (2004).

06 72. D. Laskowska, A. Berbec, Preliminary study of the newly discovered tobacco species
07 *Nicotiana wuttkei* Clarkson et Symon. **50**, 835–839 (2003).

08 73. F. Lemoine, D. Correia, V. Lefort, O. Doppelt-Azeroual, F. Mareuil, S. Cohen-Boulakia, O.
09 Gascuel, NGPhylogeny.fr: new generation phylogenetic services for non-specialists. *Nucleic
10 Acids Res.* **47**, W260–W265 (2019).

11 74. S. Heritage, “MBASR: Workflow-simplified ancestral state reconstruction of discrete traits
12 with MrBayes in the R environment” (preprint, Bioinformatics, 2021), ,
13 doi:10.1101/2021.01.10.426107.

14 75. F. Huber, L. Ridder, S. Verhoeven, J. H. Spaaks, F. Diblen, S. Rogers, J. J. J. van der Hooft,
15 Spec2Vec: Improved mass spectral similarity scoring through learning of structural
16 relationships. *PLOS Comput. Biol.* **17**, e1008724 (2021).

17 76. A. Weinhold, I. T. Baldwin, Trichome-derived O-acyl sugars are a first meal for caterpillars
18 that tags them for predation. *Proc. Natl. Acad. Sci.* **108**, 7855–7859 (2011).

19